



UNIVERSITY OF CRETE

PHYSICS DEPARTMENT

MSc THESIS

---

# Design of a Laser Frequency Stabilization Module for Space Applications

---

*Author*

Maria Georgousi

*Supervisors*

Prof. Konstantinos Makris

Dr. Wolf von Klitzing

October 2022

# Abstract

Nowadays, quantum sensors are an interesting achievement combining high level physics with sophisticated technology. Scientists conduct more and more experiments with such sensors in space, using laser techniques. One of the them is the Doppler-free saturated absorption spectroscopy, that allows for great frequency stabilization. The aim of this thesis is to present an analysis and 3D design of a module, that achieves stabilization, using the aforementioned spectroscopic method, while having low cost and small size at the same time. The analysis includes the trade-off of the optical components that are going to be used, so that the most suitable combination is chosen, based on size, reflectivity, transmittance, wavelength range, manufacturer and price criteria, among others. In addition, a significant part of the analysis is dedicated to the intensity ratio of the two beams (pump-probe), both at the detector, and the atom cell. This way, one can choose the proper lenses and non-polarizing elements, that affect the final beam ratio. A testing version is built to prove that the spectroscopy configuration actually works, and the desired signal is presented. The preliminary design is included with the most important features, as created in Inventor (*Autodesk 2021*). At a later stage, it is to be used for the manufacturing of the final module, through the 3D printing technique.

**Keywords:** *lasers – frequency stabilization – Doppler effect – spectroscopy:saturated absorption – space – 3D printing – module – design*

# Acknowledgements

I would like to thank my supervisors, Dr. Wolf von Klitzing, for the guidance, help, cooperation and support to carry through with the current project, and also Prof. Konstantinos Makris for his valuable input. Moreover, I am thankful to my colleagues at Cretan Matter Waves Group and Space Optics lab at Institute of Electronic Structure and Laser (F.O.R.T.H.), for their help and advice, that proved crucial for the development of this project. Special thanks to those who helped with the 3D printing of the mock-up. Lastly, I would like to thank my family, friends and all my beloved ones for their support and encouragement.

# Contents

<b>1</b>	<b>Laser Principles</b>	<b>7</b>
<b>2</b>	<b>Laser Spectroscopy</b>	<b>9</b>
2.1	Properties of Rubidium . . . . .	9
2.2	Spectral line broadening . . . . .	9
2.3	Saturated absorption spectroscopy . . . . .	10
2.4	Basic arrangement . . . . .	11
<b>3</b>	<b>Components</b>	<b>12</b>
3.1	Setup drawings . . . . .	12
3.2	Components list . . . . .	14
3.3	Components trade-off analysis . . . . .	15
3.3.1	Fiber Coupler . . . . .	15
3.3.2	Rb atom cell . . . . .	15
3.3.3	Photodiode . . . . .	16
3.3.4	Quarter waveplate . . . . .	17
3.3.5	Mirror . . . . .	18
3.3.6	Lens . . . . .	18
3.3.7	Amplifier/Photodetector . . . . .	19
3.3.8	Plate Beamsplitter . . . . .	20
3.3.9	Polarizing Beamsplitter . . . . .	20
3.3.10	Non-polarizing Beamsplitter . . . . .	20
3.4	Budget Overview . . . . .	22
<b>4</b>	<b>Computational analysis and results</b>	<b>23</b>
4.1	Project Analysis Flow Graph . . . . .	23
4.2	Reflectivity and Transmittance Error Distributions . . . . .	25
4.3	Error distribution analysis . . . . .	25
4.3.1	Intensity distribution - setup no.1 . . . . .	25
4.3.2	Intensity distribution - setup no.2 . . . . .	29
4.4	Reflectivity and Transmittance Measurements . . . . .	33
4.5	Calculated Intensity Results . . . . .	33
4.5.1	Intensity - setup no.1 . . . . .	33
4.5.2	Intensity - setup no.2 . . . . .	34
4.6	Lenses specifications . . . . .	34
4.7	Lens distance analysis . . . . .	34
4.7.1	Calculated Lens distance - setup no.1 . . . . .	35
4.7.2	Calculated Lens distance - setup no.2 . . . . .	35
4.8	Results and Discussion . . . . .	36
4.8.1	Limitations on the distance . . . . .	36
4.8.2	Updated distance cases . . . . .	36
4.9	Magnetic field modulation analysis . . . . .	38
<b>5</b>	<b>Setup testing version</b>	<b>40</b>
5.1	Design of testing version . . . . .	40
5.2	Manufacturing of testing version . . . . .	41
5.3	Results . . . . .	42
<b>6</b>	<b>3D Module Design</b>	<b>46</b>
6.1	Additive Manufacturing technique . . . . .	46

6.1.1	Materials . . . . .	46
6.1.2	Processes . . . . .	46
6.1.3	3D printing in space . . . . .	47
6.2	Computer-Aided Design (CAD) . . . . .	47
6.3	Setup Dimensions . . . . .	48
6.4	Project Design and Prototyping Flow Graph . . . . .	48
6.5	3D Setup . . . . .	50

# Introduction

Lasers are probably one of the most important inventions in the field of atomic physics, while having a great variety of applications in many more fields, as well. At the same time, space industry grows more and more over the past decades, with the space projects making use of new technological techniques. As one might expect, many space projects have used, and will continue to use lasers, as part of their scientific payload, their communication systems and many more. In addition, quantum technologies become more important, and in most cases, one needs to address atoms with certain wavelengths. Specifically, there are plenty new projects that bring ultracold atoms into space, such as *OBST* and *STE-QUEST*, and for that, laser frequency stabilization is needed more than ever. The solution to this is given by matter wave physics, namely the saturated absorption spectroscopy. By using particles, such as Rubidium atoms, and taking advantage of the Doppler effect due to their motions, one can actually derive a signal, which can be very stable, and lock the laser at the preferred frequency.

There are already optical arrangements studied, that achieve frequency stabilization, and they will not be studied thoroughly here. However, it is interesting to develop a miniaturized version of them, so that they can be used in space applications, as part of bigger space experiments, on satellites, or the space industry. The aim of the current thesis is to study and present a design of a module, herein referred to as setup, with small dimensions, and low cost, suitable for space projects. The design will be realized using 3D-printing techniques at a later stage, so the whole analysis is headed to this direction. At this point, it is noted that Additive Manufacturing is really important and effective in industry fields, when it comes to low cost, mass production, precision and rapid prototyping.

The current project aims at manufacturing a new 3D printed module, using innovative laser spectroscopy techniques, and could later be used as a reference for space grade models. Similar experiments have been conducted in the past, such as [5] and [6], but in our case, the setup is much smaller and compact, costing less. However, the most significant advantage is that it offers a ready spectroscopy arrangement (working for any alkali atoms), that anyone can use in a quick, simple way, by integrating it to their system. Hopefully, this setup can later be used in industry and become commercialized, so that one can easily buy it without having a great deal of calculations and work to do. In short, this prototype is an excellent idea for space applications, but will certainly be useful for portable ground-based atom quantum sensors. However, before moving on to the 3D printed module, a testing version is produced, using space-qualified materials, in order to prove that the selected spectroscopy configuration delivers the desired results.

In short, the theory for the laser mechanism is presented in chapter 1, whereas the basic spec-

troscopy knowledge in chapter 2. The components trade-off analysis is presented in chapter 3, and the computational analysis in chapter 4. Lastly, the integration of the testing version and the 3D design are presented in chapter 5 and chapter 6, respectively.

# Chapter 1

## Laser Principles

Lasers are a modern technology achievement, with many applications, and great importance in various physics and industry fields, such as laser welding, cutting, engraving or spectroscopy. Their predecessors are called *Masers*, which stands for **M**icrowave **A**mplification by **S**timulated **E**mission of **R**adiation. Masers are devices that produce electromagnetic waves in the radiowave part of the spectrum, by amplifying the stimulated emission of the atoms in the gain medium. They were first studied in 1953 by Charles H. Townes, James P. Gordon and Herbert J. Zeiger. They are commonly used in atomic clocks and in radio telescopes. Some years later, in 1960, lasers were demonstrated for the first time at Hughes Research Laboratories, by Theodore H. Maiman. This name is also an acronym, meaning "**L**ight **A**mplification by **S**timulated **E**mission of **R**adiation". The main difference with masers lies in the fact that lasers produce electromagnetic waves closer to the visual part of the spectrum ([8]).

Lasers' and masers' functionality is based on stimulated emission of the gain medium atoms. Initially, we assume that an atom is at the upper level  $n'$ . Then, an electromagnetic wave - photon - with frequency  $\nu$  and energy  $h\nu$  is incoming to the material that contains the atom; then, only in case that the photon has the same frequency as the atomic frequency, it is possible that the photon will *stimulate* the atom to undergo the transition  $n' \rightarrow n$ , where  $n$  is a lower energy level. By doing so, the atom loses energy, which is emitted as a photon of energy  $\Delta E = E_{n'} - E_n$ . Most importantly, the outgoing photon has the same direction and energy as the incoming one, meaning these two are identical.

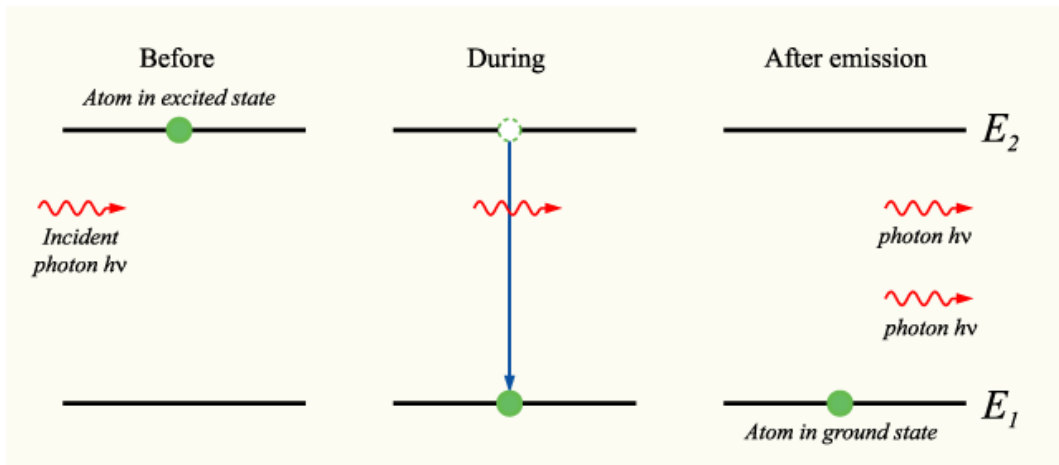


Figure (1.1) Stimulated emission mechanism



In non-thermodynamic equilibrium conditions, a material can have  $N_2 > N_1 \cdot \left(\frac{g_2}{g_1}\right)^1$ , which is exactly the opposite of the case of thermodynamic equilibrium. This phenomenon is called *population inversion*. In order to obtain a laser mechanism, we need to make this amplifier also an oscillator, by initiating and maintaining a positive feedback. This is done by inserting the active material inside a resonant cavity, for example in between two mirrors with high reflectivity. Then, the photons travel between the mirrors, as they are reflected back into the gain region, which amplifies them. In addition, if one mirror is partially transparent, then one takes an output beam from it, which is the known *laser beam*.

Lastly, the lasers used for such kind of experiments (e.g. spectroscopy) have four basic properties:

1. Monochromaticity: As the oscillation happens inside the cavity, the emitted radiation can only have the resonance frequencies of it, leading to a much narrower linewidth for the atomic transitions.
2. Coherence: There are two kinds of coherence: spatial and temporal; in spatial coherence, the points that are in the same wavefront of an electromagnetic wave have the same phase at any time  $t > 0$ . In temporal coherence, for the same point at two different moments  $t$ ,  $t + \Delta t$ , the phase difference remains the same.
3. Directionality: Again, due to the fact that lasers are based on the existence of the aforementioned resonant cavity, they appear to have great directionality. This means that the beam has reduced divergence and is then *diffraction limited*.
4. Brightness: In general, it is the power emitted by a source, per unit area and per unit solid angle. Lasers have many orders of magnitude greater brightness than usual sources.

---

<sup>1</sup> $N_1, N_2, g_1, g_2$  are the atom populations, and the statistical weights of levels 1 and 2 respectively.

# Chapter 2

## Laser Spectroscopy

### 2.1 Properties of Rubidium

Rubidium is a good option for saturated absorption spectroscopic experiments, for many reasons; it is an alkali metal, found in nature as an isotopic mixture of 72%  $^{85}\text{Rb}$  and 28%  $^{87}\text{Rb}$  [1]. Its melting and boiling points are at  $39^\circ\text{C}$  and  $688^\circ\text{C}$ , respectively, meaning that one can use cells with Rb vapour at room temperature. Also, its transition lines, especially D-lines, can be reached by tunable diode lasers and the sub-transitions are appropriate for laser cooling. In particular, the transitions we are interested in are  $5\text{S} \rightarrow 5\text{P}$ , where 5P is split into  $5P_{1/2}$  and  $5P_{3/2}$ , due to spin-orbit coupling (*fine structure*). In this project, only the second transition, which corresponds to the D2 line, will be studied. In addition to the fine structure, there is also the hyperfine splitting, due to the coupling of the total electron angular momentum  $\vec{J}$  with the nuclear spin  $\vec{I}$  [7]. The total atomic angular momentum is given by:

$$\vec{F} = \vec{L} + \vec{I}. \quad (2.1)$$

For the excited state of the D2 line, that we are interested in here, F can take any of the values 0, 1, 2, or 3.

### 2.2 Spectral line broadening

Spectral lines are not described by delta functions, as there is broadening, caused by different mechanisms: natural broadening, due to finite lifetime of the upper level, that gives us  $\Gamma \cong 6\text{MHz}$  for Rb, pressure broadening, due to collisions, power broadening, Doppler broadening, and many more. For this project, Doppler broadening, which is due to the thermal motion of the emitting atoms, will be studied.

On the Doppler effect, we consider that an atom with velocity  $v$  interacts with a photon with frequency  $\omega$ . When in rest, atoms in a gas normally absorb radiation only with  $\omega = \omega_0$ , so when the atom has the aforementioned velocity, it absorbs as:

$$\frac{\omega - \omega_0}{\omega_0} = \frac{v}{c}. \quad (2.2)$$

Eventually, the Doppler-broadened line has a full width at half maximum (FWHM) equal to

$$\frac{\Delta\omega_0}{\omega_0} = 2 \cdot \sqrt{\ln 2} \cdot \frac{v}{c}, \quad (2.3)$$

which, for Rb atom gas, is  $\Delta\omega_{Doppler} \sim 500 \text{ MHz} \gg \Gamma$ . This is why the final signal is dominated by the Doppler line broadening contribution at room temperature. In the next section, we will see how one can get rid of this, and achieve Doppler-free spectroscopy.

## 2.3 Saturated absorption spectroscopy

Saturated absorption spectroscopy is a method that allows us to measure precisely the transition frequency of an atom between two levels (one of them usually is the ground state). This happens because it eliminates the Doppler broadening effects, without even changing the room temperature. This method is also used for laser locking in atomic physics experiments.

The main idea is based on the pump-probe scheme; there is a strong beam, called *pump*, which is  $\sim 95\%$  of the input experiment laser beam, that comes into the vapor cell. Then, through some arrangements using optical components, a second weak beam (that is the remaining  $\sim 5\%$  of the laser beam) with the same frequency is also sent through the cell, in a counter-propagating way [3].

In the case of only one beam, let us say the probe, while scanning the laser frequency, atoms absorb energy from the incident laser photons only when the probe frequency  $\omega$  is equal to the atomic resonance frequency  $\omega_0$ , that is  $\omega = \omega_0$ . The absorption profile is then *Doppler broadened*. If we add the second beam, in our case, the pump beam, there is a small peak at the atomic resonance. The reason for this is simple, and is given next.

In the case of  $\omega_0 - \Delta\omega < \omega_{laser} < \omega_0 + \Delta\omega$ <sup>1</sup>, atoms that participate in the probe absorption are the ones that moves towards the probe beam (in an opposite direction) (blue-shift Doppler effect), whereas all other atoms, that have velocities not in the same direction with the probe, remain unaffected. The atoms that can "see" the probe beam as blue-shifted, can also see the pump beam red-shifted, as it moves on exactly the opposite direction as the probe beam. The inverse happens for the atoms having velocity equal to  $-v$ . So, the pump beam does not affect the probe absorption, in the case where  $\omega \neq \omega_0$ .

In the case where  $\omega = \omega_0$ , only the atoms with  $v = 0$  can "see" both the pump and probe beams on resonance, resulting in a peak in the transmission spectrum of the absorption probe profile. A dip is then created in the output intensity of the profile, which is called *Lamb Dip*, that has a linewidth close to that of the initial transition.

When there is a system with more than one atomic excited states, for example two, that have a separation less than the Doppler width  $\Gamma$ , there are ultimately three resonance frequencies observed;  $\omega_1$  for the first state,  $\omega_2$  for the second state, and the *cross-over* resonance

$$\omega_{resonance} = \frac{\omega_1 + \omega_2}{2}. \quad (2.4)$$

By subtracting the signal from the two beams, one can get rid of the background Doppler broadened signal. Moreover, if we take advantage of the Zeeman effect, by modulating the magnetic field of the atoms, we can get an even clearer signal. Using a lock-in amplifier, which consists of a DC amplifier, a frequency mixer and a low-pass filter, the derivative of the absorption signal is obtained, which is called *error signal*, and is the desired final result of this method.

---

<sup>1</sup> $\Delta\omega$  is the laser detuning

## 2.4 Basic arrangement

The following figure presents a basic, simple arrangement of optical components, suitable for Doppler-free spectroscopy.

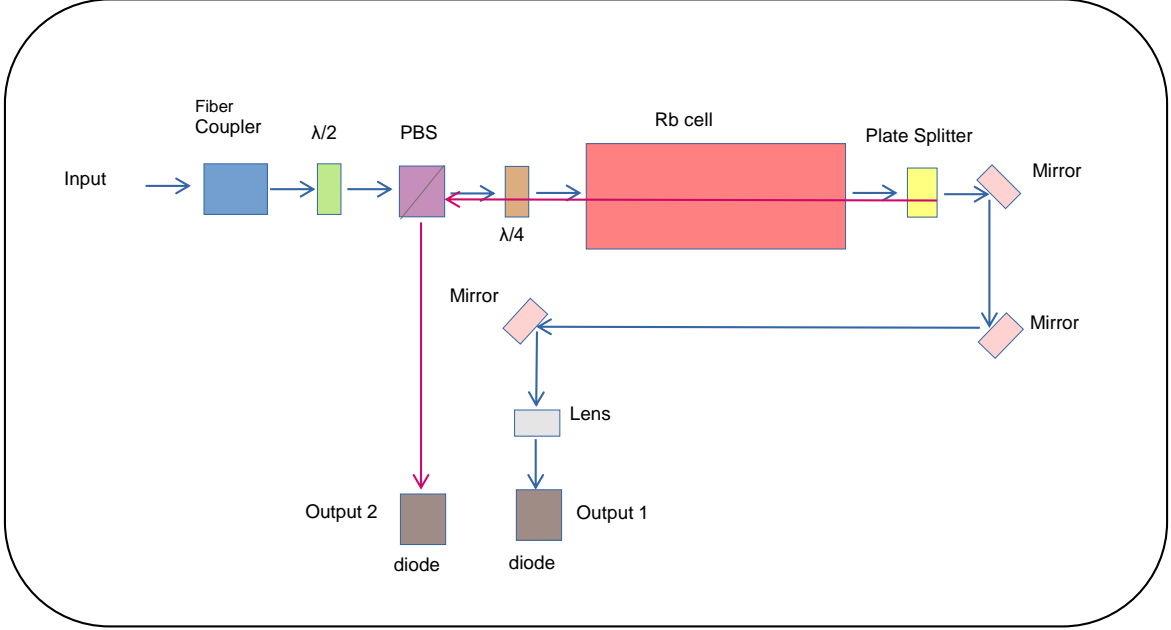


Figure (2.1) Doppler-free spectroscopy arrangement (based on [2])

For better understanding, the Polarizing Beamsplitter (PBS), together with the half waveplate, controls the intensity of the laser beam, that is used for the rest of the experiment. The beam then goes through the atom vapor cell, after passing through a quarter waveplate and changing its polarization from linear to circular. Then, the Beam Sampler (BS), or Plate Beamsplitter, splits the beam into two, the aforementioned pump and probe. They are then measured at the detector, after being reflected to several mirrors. At this point, it is important to note the existence of a lens at the optical path of the pump beam, right before the detector. (section 3.3.6).

# Chapter 3

## Components

In this chapter, the process of the component trade-off analysis and selection is followed.

### 3.1 Setup drawings

Doppler-free saturated absorption spectroscopy using Rubidium atoms (chapter 2) is, as already mentioned, a usual technique used for laser locking - or laser frequency stabilization, where the laser signal consists of pulses with very short duration. Based on fig. 2.1, a pretty compact and simple way to build such an arrangement is shown in fig. 3.1 (some changes have been made due to the small-scale nature of this project).

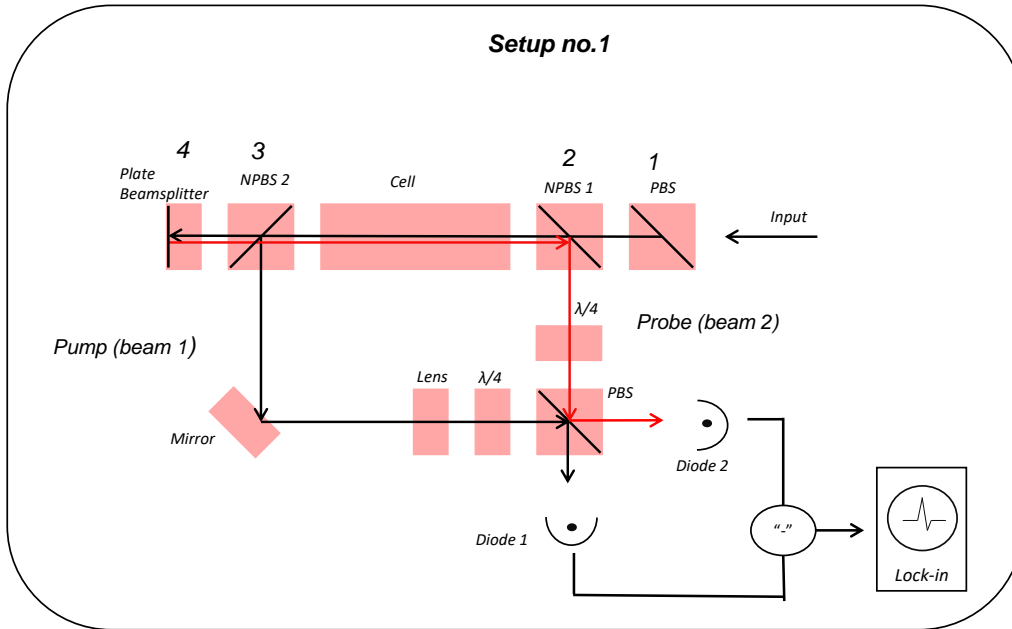


Figure (3.1) Drawing no.1

The input laser beam enters the system through the Fiber Coupler (not shown here) from the

right side. Then, a PBS cleans up the polarization, and the first NPBS divides the beam, and the pump probe is transmitted through the Rb cell. The second NPBS reflects the pump beam to the mirror, the lens, the quarter waveplate, and finally, through another PBS, to the photodetector (at both outputs). The transmitted beam from the second NPBS is partially reflected from the Plate Beamsplitter, creating the probe beam (red line). It is then guided again through the cell, reflected by the first NPBS, and through a quarter waveplate and a PBS, arrives at the photodetector (at both outputs).

After some analysis, it was found that a similar, and probably more convenient setup is shown in fig. 3.2:

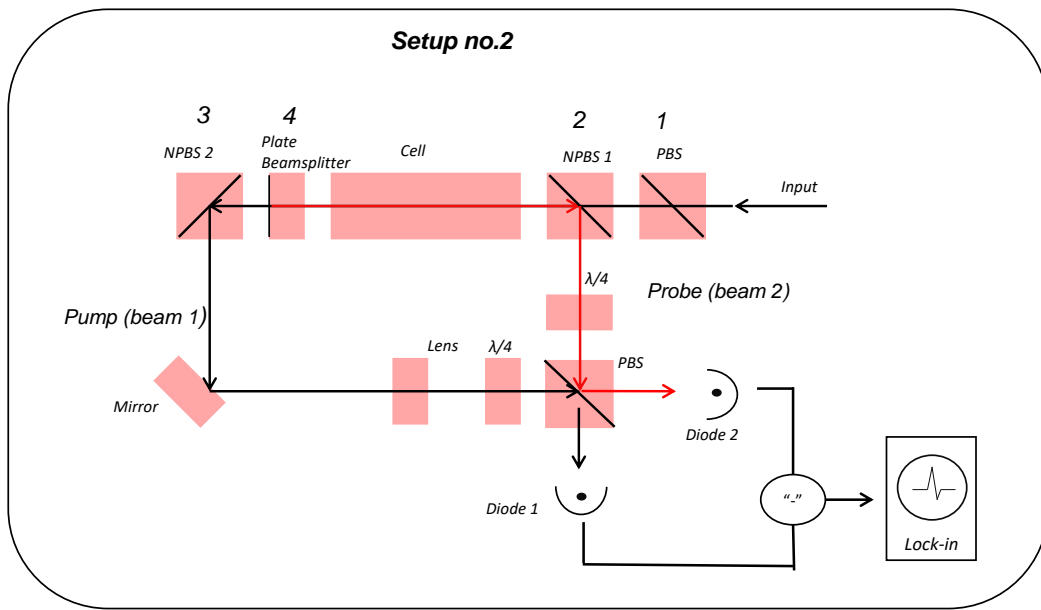


Figure (3.2) Drawing no.2 - It is the same as Drawing no.1, except for the position switch between the second NPBS and the Plate Beamsplitter

where the only difference is that the second Non-Polarizing Beamsplitter and the Plate Beamsplitter switch places. This scenario appears far more promising, as the initial beam is split into pump and probe right after the cell (by the Plate Beamsplitter), and the optical path becomes much simpler than in the first setup, where the probe beam is transmitted through the second NPBS too. The two beams are shown with different colors: red for the probe beam and black for the pump beam. The waveplates and the second PBS are used in order to change the polarization from linear to circular and both beams will be detected at both outputs ( $\sigma$  and  $\pi$  polarization). In the course of this thesis, pump beam will often be referred to as *beam 1* and probe beam as *beam 2*. Moreover, *Input* describes the point where the signal from the main laser source is coupled.

A third setup was developed during the initial project stages. As shown below, it is a very simplified version of the two previous setups, containing only a PBS (for clear polarization),

the cell, a quarter waveplate and a Plate Beamsplitter for creating the two beams. It will be studied at a later time, and it is not further mentioned in this project.

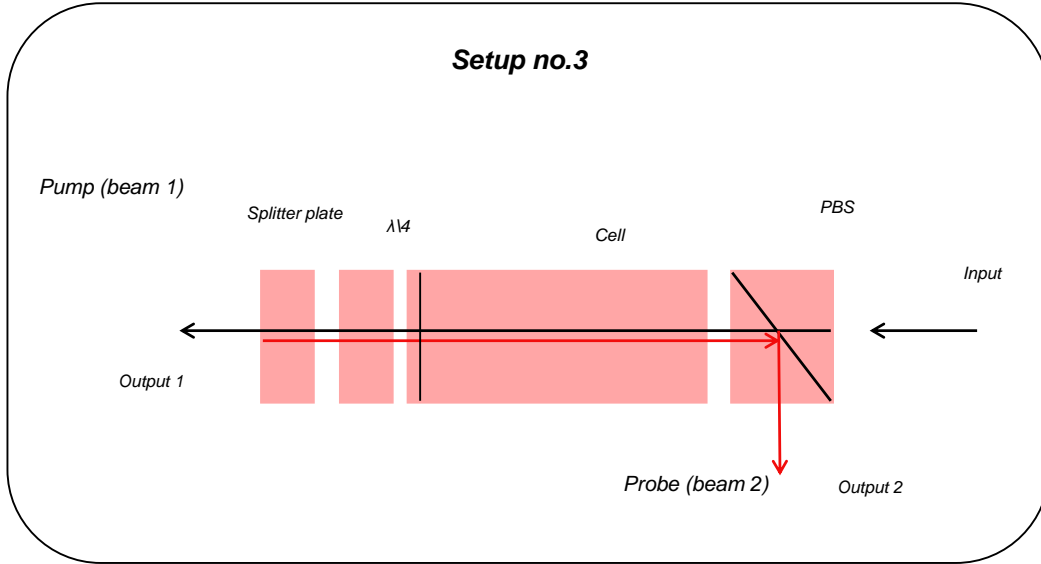


Figure (3.3) Setup no.3

Briefly, fig. 3.1 and fig. 3.2 are the two sketches of the final setups, that will be studied in this thesis, and will be referred to as ***Drawing no.1*** and ***Drawing no.2*** respectively, from this point on.

## 3.2 Components list

As mentioned before, the main goal of this project is to deliver a final 3D printed setup, for laser frequency stabilization, using laser spectroscopy techniques. The most important advantage of this scheme is the small cost and size, which make the setup most appropriate for space applications. However, in order to achieve this, one must design the model with great accuracy, meaning that has to decide on the components on an early stage, and include all the characteristics and specifications in the design.

In short, the components list is presented below:

Component	Quantity
Fiber Coupler	1
Rb atom cell	1
Photodiode	2
Quarter waveplate	2
Mirror	1
Lens	1
Amplifier	1
Plate Beamsplitter	1
Polarizing Beamsplitter (PBS)	2
Non-polarizing Beamsplitter (NPBS)	2

Table (3.1) Components list

### 3.3 Components trade-off analysis

In section 3.3.1 - section 3.3.10, the trade-off analysis and tables will be presented, and the final components with specific part numbers will be selected.

#### 3.3.1 Fiber Coupler

The fiber coupler is an optical device used on fibers, in order to pair/couple the light from one or more input fibers, to one or more output fibers. In the current experiment, we need to integrate the laser beam from the lab's main laser in the setup, so that we have a laser beam as the input signal.

Table (3.2) Trade-off table for Fiber Coupler

Part number	F220APC-780	F230APC-780	F260APC-780	F280APC-780	60FC-4-A8-07
Company	Thorlabs	Thorlabs	Thorlabs	Thorlabs	Schafter & Kirchhoff
Wavelength	780 nm	780 nm	780 nm	780 nm	650 - 1150 nm
Type	FC/APC	FC/APC	FC/APC	FC/APC	FC/APC
Focal length	11.07 mm	4.51 mm	15.29 mm	18.40 mm	8.00 mm
Price	208.00 €	208.00 €	208.00 €	208.00 €	344.00 €
Comments	Small beam	Small beam	Small beam	-	Expensive
Selected	No	No	No	Yes	No

As one can see from table 3.2, the best choice is the coupler **F280APC-780**, from Thorlabs. It contains an aspheric lens and its type is FC/APC - which stands for *Fiber Channel / Angled Physical Contact*, meaning that it couples with a fiber having an angled endface radius, in order to minimize back reflection. This will also create a laser beam diameter equal to  $3\text{ mm}$ , which is important here.

#### 3.3.2 Rb atom cell

In Rubidium saturated-absorption spectroscopy arrangements, Rb-atom cells are used, offering a unique absorption profile. In our case, the cell must be as small as possible, and unfortunately,



the components available in the market do not have great variety. Previous projects that took part in our lab showed that Triad Technology Inc. offers good solutions to such problems, so no trade-off analysis was done, and the following component was selected:

Table (3.3) Rb atom cell specifications

<b>Part Number</b>	<b>TT-RBX10X20-QW</b>
<b>Dimensions</b>	10mm x 20mm
<b>Atom type</b>	Rubidium Rb-87
<b>Cell type</b>	Quartz



Figure (3.4) The Rb atom cell TT-RBX10X20-QW compared to a 20-cent coin

It is apparent that the cell size is really what makes this project different and miniaturized. Most of the very small components used here, such as photodiodes, or waveplates, are also used in conventional spectroscopy configurations of normal size. This is the difference, however, with the selected Rb cell.



Figure (3.5) The selected Rb cell (top), compared to a usual one (bottom)

### 3.3.3 Photodiode

The output signal (which corresponds to the probe beam signal and the pump beam signal), will be detected through two pin photodiodes. After some study, the following table presents the trade-off analysis for the photodiode.

Table (3.4) Trade-off table for Photo diode

Part Number	<b>PNZ300-ND</b>	<b>SFH 213</b>	<b>TEMD1030</b>	<b>BPW83</b>
Company	Panasonic	OSRAM/Mouser	Vishay	Vishay
Material	Silicon	Silicon	Silicon	Silicon
Lens	Yes	Yes	Yes	No
Wavelength	800 nm	850 nm	790-1050 nm	950-1050 nm
Comments	Available at the lab - not manufactured anymore	Needs ordering	Surface mount	No lens, more expensive, needs ordering
Selected	Yes	No	No	No

As one can see, the best solution is the **PNZ300-ND** model, as there are already plenty of them in the lab, and it seems to satisfy the material, wavelength and lens criteria. As a note, prices are very low and similar, and they are not included in this table.

### 3.3.4 Quarter waveplate

As shown in fig. 3.1 and fig. 3.2, two quarter waveplates are necessary for the spectroscopy setup. In general, this kind of waveplates is used in order to turn linearly polarized light into circularly polarized light. Below we can see the available models and the trade-off analysis done during this project:

Table (3.5) Trade-off analysis for Quarter Waveplate

Part number	<b>05RP34-780</b>	<b>WPQ05M-780</b>	<b>WPQ05ME-780</b>	<b>464-4420</b>	<b>WPF4210-780</b>
Company	Newport	Thorlabs	Thorlabs	Eksma	Union
Wavelength	780 nm	780 nm	780 nm	780 nm	780 nm
Type	Zero-order	Zero-order	Zero-order	Zero-order	True zero-order
Diameter	12.7 mm	12.7 mm	12.7 mm	17 mm	10 mm
Mount	Yes	Yes	Yes	Yes	No
Price	832.00 €	430.00 €	247.00 €	310.00 €	60.00 €
Comments	Expensive	Mount to big	-	-	Already available at the lab, true zero-order instead of zero-order
Selected	No	No	No	No	Yes

From the above, we can see that model **WPF4210-780** is the best choice, as it was already purchased and available at a great number at the lab, and it is a true zero-order waveplate, as well. In this point, it is important to mention that zero-order waveplates consists of two Quartz plates that are contacted together with their optical axes forming a right angle. True

zero-order waveplates are basically the ideal case of zero-order ones, because they offer great accuracy.

### 3.3.5 Mirror

One of the most common optical component type used in setups is the mirror. Here, from fig. 3.1 and fig. 3.2, we see that there is need for one mirror in order to distinguish between the two optical paths of the pump and the probe beams. The most suitable models found for this aim are presented and compared below:

Table (3.6) Trade-off analysis for Mirror

Part Number	BB05-E03	031-0780T6
Company	Thorlabs	Eksma
Wavelength	750-1100 nm	780 nm
Type	Broadband, dielectric	Laserline, BK7 substrate
Diameter	12.7 mm	12.7 mm
Price	43.4 €	63.00 €
Selected	Yes	No

From the above, model **BB05-E03** seems to be the best option, as its wavelength range is wider, has appropriate dimensions and can be ordered from the same company as the rest of the components.

### 3.3.6 Lens

In order to have the right detected signal for the saturated absorption spectroscopy, or in other words, to be able to subtract the two beams' signals, we need to have the same intensity for the two beams, probe and pump at the detector (or equivalently, at the second PBS). In order to achieve this, a lens is required, in order to increase the pump beam diameter, and so, its intensity to decrease (according to inverse square law) (fig. 4.14). This is possible with a plano-concave or bi-concave lens, due to its shape. The following models were included in the trade-off analysis:

Table (3.7) Trade-off analysis and specs for Lenses

Part Number	LC1060-B	SLB-12.7-30NIR2	LD2568-B	LD2060-B	LD1357-B	LD2746-B
Company	Thorlabs	Optosigma	Thorlabs	Thorlabs	Thorlabs	Thorlabs
Focal length	-30mm	-30mm	-9mm	-15mm	-50mm	-6mm
Wavelength	650-1050 nm	750-1550 nm	650-1050 nm	650-1050 nm	650-1050 nm	650-1050 nm
Dimensions	12.7 mm	12.7 mm	9 mm	12.7 mm	12.7 mm	6 mm
Coating	AR	AR	N-SF11	N-SF11	N-BK7	N-SF11
Price	27.22 €	44.10 €	35.54 €	38.31 €	32.76 €	35.54 €
Comments	Plano-concave	Plano-concave	Bi-concave	Bi-concave	Bi-concave	Bi-concave
Selected	No	No	Yes	Yes	Yes	Yes

As the lens selection depends mainly on the ratio of the two beams, and subsequently on the rest of the components, four of the them were purchased in order to cover every case. The lens selection analysis will be presented in section 4.7

### 3.3.7 Amplifier/Photodetector

For the current project, the output signal is the primary result one expects. In order to obtain it, photodiodes (section 3.3.3) need to connect to an amplifier, and most preferably, to a transimpedance one. This device is a current to voltage converter, which in turn amplifies the output current with a linearity better than 1%, when specifically connected to photodiodes. Two possible models were considered in our case:

Table (3.8) Trade-off analysis for Amplifier/Photodetector

Part Number	PD10TIA-80-DC	PDX10B-80-DC-SI
Company	Koheron	Koheron
Dimensions	63x38x14mm	49x40x18mm
Gain	80 kV/A	80 kV/A
Noise (1 MHz, 50 $\Omega$ )	0.8pA/ $\sqrt{Hz}$	1.4pW/ $\sqrt{Hz}$
Price	155.00	325.00
Comments	Less noice, better diode arrangement	Bigger, needs extra components
Yes/No	Yes	No

Model **PD10TIA-80-DC** seems the best choice for our case, as it has a low input-referred current noise, and its structure allows two diodes to connect in a right angle in an easier way, as shown in fig. 3.1 and fig. 3.2. As it is to be integrated in the setup at a later stage, it is not yet purchased and tested in the course of this thesis.

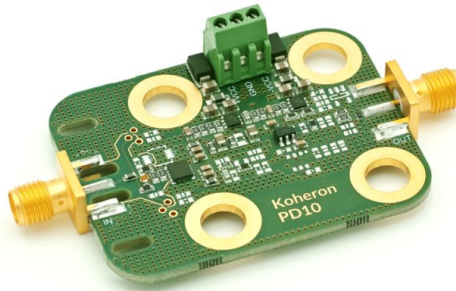


Figure (3.6) The transimpedance amplifier PD10TIA-80-DC

At this point, it is important to note the significance of being able to obtain such circuits nowadays, without having to study and build one from scratch.

### 3.3.8 Plate Beamsplitter

The plate beamsplitter is one of the most important components in the project, as it is the one that separates the initial laser beam, into the pump and probe beams. The difference of the two beams needs to be as great as possible inside the Rb atom cell, so plates with a ratio R:T = (10:90) are preferred, as they are the ones in the market with the lowest Reflectivity.

Table (3.9) Trade-off analysis for Plate Beamsplitter

Part Number	BSN04	BSN05
Company	Thorlabs	Thorlabs
Diameter	12.7mm	12.7mm
Wavelength	400-700 nm	700-1100 nm
R:T	10:90	10:90
Coating	AR	AR
Price	90.74 €	90.74 €
Comments	Wavelength range not accurate	-
Yes\No	No	Yes

Due to better wavelength range, model **BSN05** is the best choice. The plate beamsplitter needs to be put in the module with great accuracy, so that the two beams overlap as much as possible, and the calculated manufacturing tolerance is  $\sim 2^\circ$ , if the dimensions of the components and the spacings between them are taken into account.

### 3.3.9 Polarizing Beamsplitter

Polarizing Beamsplitters (*PBS*) are used to separate the s- and p- components of the beam, by reflecting the s- component by  $90^\circ$ . Because this is quite simple, no trade-off analysis was conducted, and the following model was chosen, already available at the lab:

Table (3.10) Specifications of Polarizing Beamsplitter model

Part Number	PBS0012-780
Company	Union-Optic
Diameter	12.7mm
Wavelength	780-810 nm
Material	BK7
Coating	AR
Price	155.00 €
Comments	Good choice, already available at the lav

### 3.3.10 Non-polarizing Beamsplitter

Non-polarizing beamsplitters (NPBS) separate the initial beam into two new beams, by reflecting a percentage (R%) by  $90^\circ$ . This R% defines the model of the NPBS that one chooses. In our design, 2 NPBS are necessary, either with the same, or different reflectivity. However, as the models in the market have an error in Reflectivity (R%) and Transmittance (T%), and this can affect the Pump/Probe intensity ratio by a great factor, one should know the actual values

of R and T, before deciding on the best NPBS combination, and thus, on the lens. For these reasons, it was considered wiser to purchase various NPBS with different R%, and finish the design, after the measurement of R% and T% of each component. The table below includes all the available cubic NPBS, that were initially considered as possible choices:

<b>Part Number</b>	<b>BS011</b>	<b>BS038</b>	<b>BS050</b>	<b>BS059</b>
<b>Company</b>	Thorlabs	Thorlabs	Thorlabs	Thorlabs
<b>Dimensions</b>	10 mm	10 mm	10 mm	10 mm
<b>Wavelength</b>	700-1100 nm	700 -1100 nm	700-1100 nm	700-1100 nm
<b>R:T</b>	50:50	10:90	30:70	70:30
<b>Price</b>	174.42 €	174.42 €	174.42 €	174.42 €
<b>Comments</b>	Unmounted	Unmounted	Unmounted	Unmounted

However, the case with the BS011 beamsplitter, with (R:T)=(50:50) does not offer any distinction between the two beams, but only splits the initial beam into two, of equal intensity, so it was rejected before the ordering, and was not used in the analysis in chapter 4. Again, tolerances were calculated to be  $\sim 50\mu m$ , and  $\sim 2^\circ$ .

### 3.4 Budget Overview

A short budget analysis will be presented in this section. Taking into account the aforementioned component trade-off analysis, as well as the analysis in chapter 4, the following components are used, and were therefore purchased. Moreover, the table includes an estimation of the manufacturing cost (the testing version is not included).

Table (3.11) Components, manufacturing and overall cost

Component	Price (€)
Fiber Coupler (F280APC-780)	208.16
Mirror (BB05-EO3)	43.40
Lens (LD2568-B)	35.54
Plate Beamsplitter (BSN05)	90.74
NPBS (BS050)	174.42
NPBS (BS038)	174.42
NPBS (BS059)	174.42
Lens (LD2060-B)	38.31
Lens (LD1357-B)	32.76
Lens (LD2746-B)	35.54
Cell (TT-RBx10X20-QW)	445.00
Transimpedance Amplifier (PD10TIA)	155.00
PBS (PBS0012-780)	2 x 155.00
Quarter waveplate (WPF4210-780-M12.7)	2 x 60.00
Pin Photodiode (PNZ300-ND)	2 x 1.00
<b>Components cost</b>	<b>2,039.71 €</b>
<b>Manufacturing</b>	<b>~ 60.00 €</b>
<b>Total</b>	<b>~ 2,100.00 €</b>

# Chapter 4

## Computational analysis and results

### 4.1 Project Analysis Flow Graph

At the beginning of the project, a preliminary study was done, about the parameters of the experiment. For example, the appropriate operation wavelength and the approximate size was decided, along with the types of the components, the intensity of the beam at the cell, and the laser beam diameter. Then, a trade-off analysis was conducted for the components, in order to define specifically which ones were most suited for the project. However, their Transmittance and Reflectivity manufacturing specifications included such errors, so that it was not possible to do all the calculations precisely, and for some of the components, namely the Non-Polarizing Beamsplitters and the lenses, a variety was selected. Next, a computational analysis followed, in order to derive the distribution of the pump-over-probe intensity ratios, using the aforementioned R% and T% value ranges, including errors. So, one could have a first idea of what cases and combinations of the selected components could work better. However, once the components arrived at the lab, the precise values of R% and T% were measured, allowing for far more defined calculations. The exact intensity ratios were found, and for different NPBS combinations, the distances for all the selected lenses were calculated. This way, one ends up with specific cases (combinations of NPBS and lens) that can be included in the 3D CAD model, and later, in the 3D printed setup, for testing.



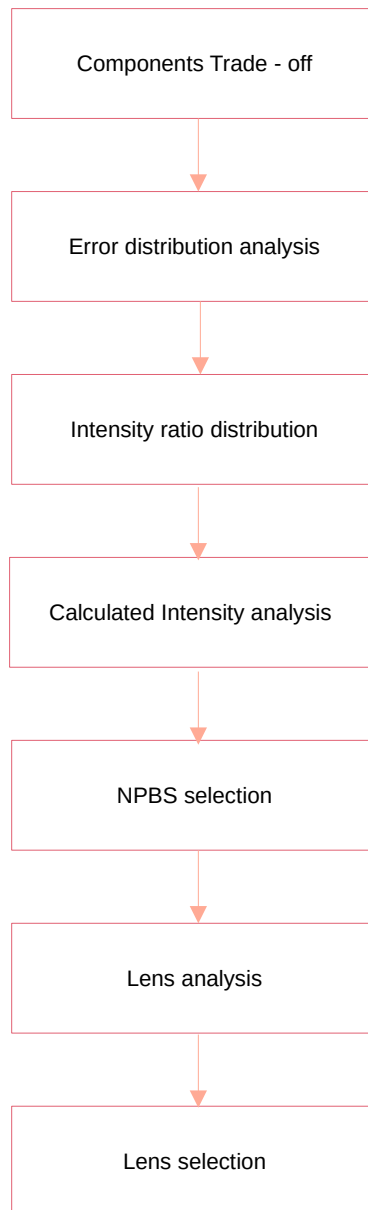


Figure (4.1) Flow graph of the project's computational analysis

## 4.2 Reflectivity and Transmittance Error Distributions

For the first part of the analysis, the error distributions of the Reflectivity (R%) and Transmittance (T%) are used, in order to define which of the possible component combinations would deliver better results, when integrated in the 3D printed setup. As seen from table 4.1, the distributions of values mentioned by the manufacturer are great, leading to uncertainties on the design. So, for this stage, only a preliminary study is possible, until the actual values are known. In particular, 6 different NPBS combinations are studied, combining two different NPBS in the two positions in fig. 3.1 and fig. 3.2 - positions 2 and 3. The purchased NPBS components (cubes and plate) are the following (section 3.3.10):

Table (4.1) NPBS - R% and T% with errors

Part Number	R	T
BS038	7 +10/-7%	87 $\pm$ 10%
BS050	27 $\pm$ 10%	62 $\pm$ 10%
BS059	67 +5/-15%	27 $\pm$ 10%
BSN05	10 $\pm$ 8%	90 $\pm$ 8%

where the R and T columns include the errors as given by the manufacturer. As it was not mentioned in the specifications, we considered a uniform distribution for the first part of the analysis. Using Python scripts in Jupyter notebooks, 100000 points were randomly selected from the aforementioned ranges, in order to obtain the results. The variables for the following equations are:

Table (4.2) NPBS variables - Symbols of parts' reflectivity and transmittance that are used in the following analysis

Part Number	R	T
BS038	Rcube10	Tcube10
BS050	Rcube30	Tcube30
BS059	Rcube70	Tcube70
BSN05	Rplate10	Tplate10

## 4.3 Error distribution analysis

In this section, the equations giving the pump/probe beam intensity ratio are derived, together with the intensity ratio distribution graphs, for every NPBS combination and for both setup cases. As a note, x-axis is in logarithmic scale (base 10), so that the difference can be more clear.

### 4.3.1 Intensity distribution - setup no.1

We begin with the study of the setup no.1, as shown in fig. 3.1, where the NPBS are in positions 2 and 3. Moreover, we denote transmittance of the PBS in position 1 as  $T_{pcube}$  and its Reflectivity as  $R_{pcube}$  (they cancel out in the equations, and so no values are needed).

### Case 30 - 10

For the first case, we consider that NPBS BS050 (with R%=30%) is in position 2 and NPBS BS038 (with R%=10%) in position 3. This way the equation giving the Intensity ratio (pump/probe) at the detector is:

$$\left(\frac{I_1}{I_2}\right)_{\text{detector}} = \frac{T_{\text{pcube}} \cdot T_{\text{cube30}} \cdot R_{\text{cube10}}}{T_{\text{pcube}} \cdot T_{\text{cube30}} \cdot T_{\text{cube10}} \cdot R_{\text{plate10}} \cdot T_{\text{cube10}} \cdot R_{\text{cube30}}}, \quad (4.1)$$

whereas the intensity ratio at the Rb cell is:

$$\left(\frac{I_1}{I_2}\right)_{\text{cell}} = \frac{T_{\text{pcube}} \cdot T_{\text{cube30}}}{T_{\text{pcube}} \cdot T_{\text{cube30}} \cdot T_{\text{cube10}} \cdot R_{\text{plate10}} \cdot T_{\text{cube10}}}. \quad (4.2)$$

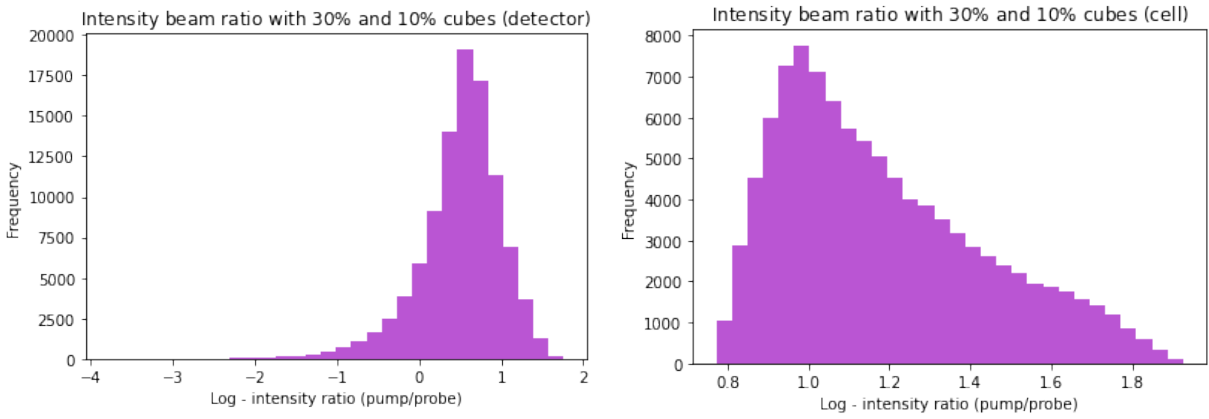


Figure (4.2) Intensity ratio (case 30 - 10)

### Case 10 - 30

For the second case, we consider that NPBS BS050 (with R%=30%) is in position 3 and NPBS BS038 (with R%=10%) in position 2. This way the equation giving the Intensity ratio (pump/probe) at the detector is:

$$\left(\frac{I_1}{I_2}\right)_{\text{detector}} = \frac{T_{\text{pcube}} \cdot T_{\text{cube10}} \cdot R_{\text{cube30}}}{T_{\text{pcube}} \cdot T_{\text{cube10}} \cdot T_{\text{cube30}} \cdot R_{\text{plate10}} \cdot T_{\text{cube30}} \cdot R_{\text{cube10}}}, \quad (4.3)$$

whereas the intensity ratio at the Rb cell is:

$$\left(\frac{I_1}{I_2}\right)_{\text{cell}} = \frac{T_{\text{pcube}} \cdot T_{\text{cube10}}}{T_{\text{pcube}} \cdot T_{\text{cube10}} \cdot T_{\text{cube30}} \cdot R_{\text{plate10}} \cdot T_{\text{cube30}}}. \quad (4.4)$$

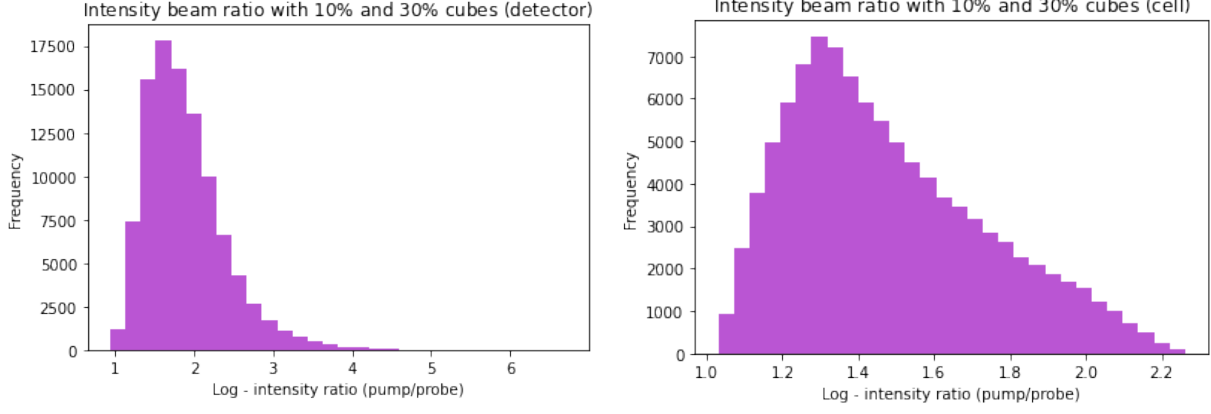


Figure (4.3) Intensity ratio (case 10 - 30)

### Case 70 - 10

For the third case, we consider that NPBS BS059 (with R%=70%) is in position 2 and NPBS BS038 (with R%=10%) in position 3. This way the equation giving the Intensity ratio (pump/probe) at the detector is:

$$\left(\frac{I_1}{I_2}\right)_{\text{detector}} = \frac{T_{\text{pcube}} \cdot T_{\text{cube70}} \cdot R_{\text{cube10}}}{T_{\text{pcube}} \cdot T_{\text{cube70}} \cdot T_{\text{cube10}} \cdot R_{\text{plate10}} \cdot T_{\text{cube10}} \cdot R_{\text{cube70}}}, \quad (4.5)$$

whereas the intensity ratio at the Rb cell is:

$$\left(\frac{I_1}{I_2}\right)_{\text{cell}} = \frac{T_{\text{pcube}} \cdot T_{\text{cube70}}}{T_{\text{pcube}} \cdot T_{\text{cube70}} \cdot T_{\text{cube10}} \cdot R_{\text{plate10}} \cdot T_{\text{cube10}}}. \quad (4.6)$$

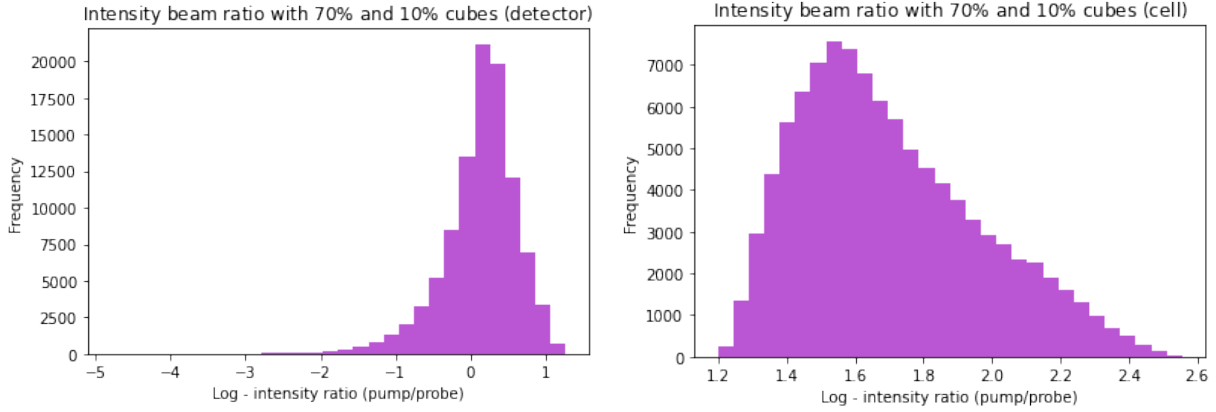


Figure (4.4) Intensity ratio (case 70 - 10)

### Case 10 - 70

For the fourth case, we consider that NPBS BS059 (with R%=70%) is in position 3 and NPBS BS038 (with R%=10%) in position 2. This way the equation giving the Intensity ratio (pump/probe) at the detector is:

$$\left(\frac{I_1}{I_2}\right)_{\text{detector}} = \frac{T_{\text{pcube}} \cdot T_{\text{cube10}} \cdot R_{\text{cube70}}}{T_{\text{pcube}} \cdot T_{\text{cube10}} \cdot T_{\text{cube70}} \cdot R_{\text{plate10}} \cdot T_{\text{cube70}} \cdot R_{\text{cube10}}}, \quad (4.7)$$

whereas the intensity ratio at the Rb cell is:

$$\left(\frac{I_1}{I_2}\right)_{cell} = \frac{T_{pcube} \cdot T_{cube10}}{T_{pcube} \cdot T_{cube10} \cdot T_{cube70} \cdot R_{plate10} \cdot T_{cube70}}. \quad (4.8)$$

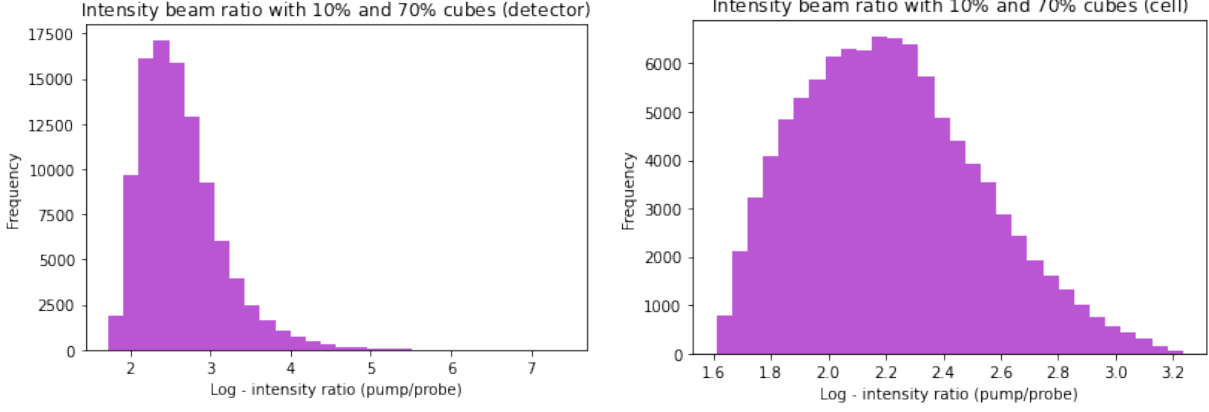


Figure (4.5) Intensity ratio (case 10 - 70)

### Case 70 - 30

For the fifth case, we consider that NPBS BS059 (with R%=70%) is in position 2 and NPBS BS050 (with R%=30%) in position 3. This way the equation giving the Intensity ratio (pump/probe) at the detector is:

$$\left(\frac{I_1}{I_2}\right)_{detector} = \frac{T_{pcube} \cdot T_{cube70} \cdot R_{cube30}}{T_{pcube} \cdot T_{cube70} \cdot T_{cube30} \cdot R_{plate10} \cdot T_{cube30} \cdot R_{cube70}}, \quad (4.9)$$

whereas the intensity ratio at the Rb cell is:

$$\left(\frac{I_1}{I_2}\right)_{cell} = \frac{T_{pcube} \cdot T_{cube70}}{T_{pcube} \cdot T_{cube70} \cdot T_{cube30} \cdot R_{plate10} \cdot T_{cube70}}. \quad (4.10)$$

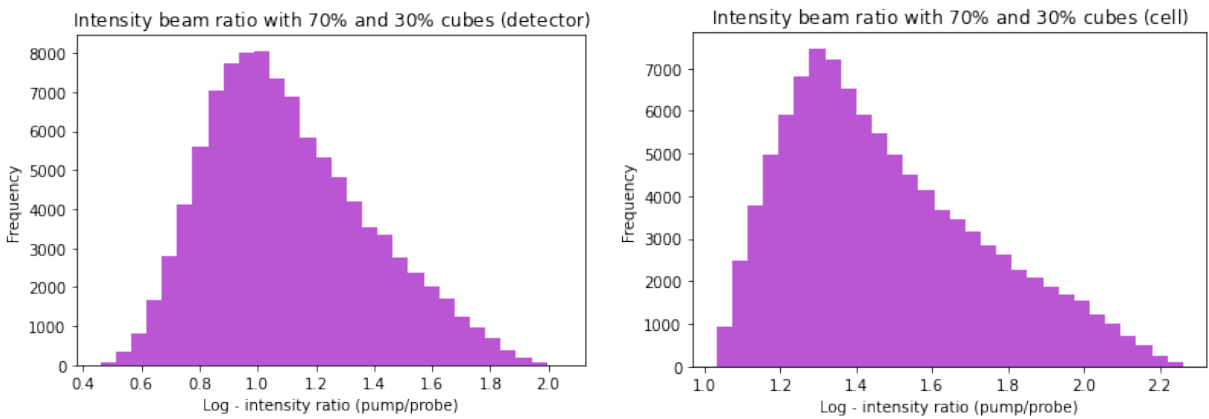


Figure (4.6) Intensity ratio (case 70 - 30)

### Case 30 - 70

For the sixth case, we consider that NPBS BS050 (with R%=30%) is in position 2 and NPBS BS059 (with R%=70%) in position 3. This way the equation giving the Intensity ratio (pump/probe) at the detector is:

$$\left(\frac{I_1}{I_2}\right)_{\text{detector}} = \frac{T_{\text{pcube}} \cdot T_{\text{cube30}} \cdot R_{\text{cube70}}}{T_{\text{pcube}} \cdot T_{\text{cube30}} \cdot T_{\text{cube70}} \cdot R_{\text{plate10}} \cdot T_{\text{cube70}} \cdot R_{\text{cube30}}}, \quad (4.11)$$

whereas the intensity ratio at the Rb cell is:

$$\left(\frac{I_1}{I_2}\right)_{\text{cell}} = \frac{T_{\text{pcube}} \cdot T_{\text{cube30}}}{T_{\text{pcube}} \cdot T_{\text{cube30}} \cdot T_{\text{cube70}} \cdot R_{\text{plate10}} \cdot T_{\text{cube70}}}. \quad (4.12)$$

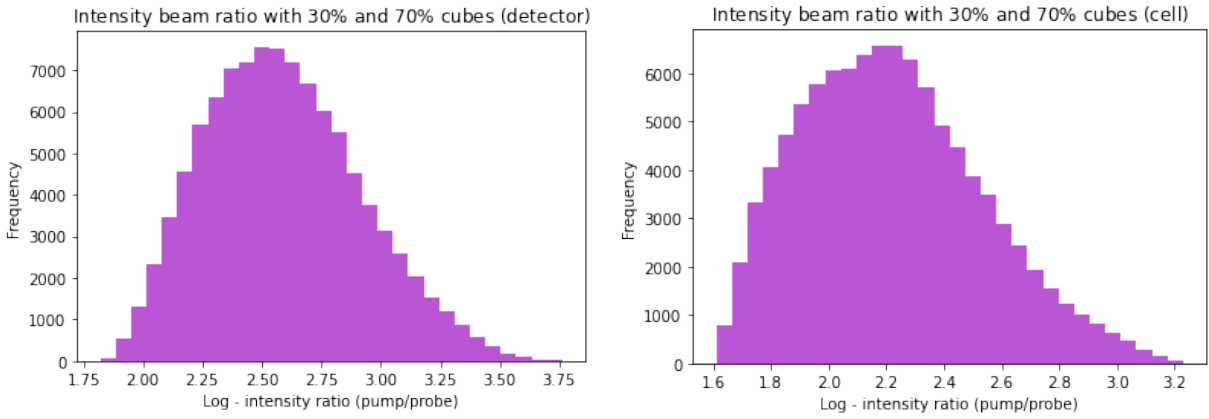


Figure (4.7) Intensity ratio (case 30 - 70)

### 4.3.2 Intensity distribution - setup no.2

The same analysis will follow for setup no.2, as shown in fig. 3.2

### Case 30 - 10

For the first case, we consider that NPBS BS050 (with R%=30%) is in position 2 and NPBS BS038 (with R%=10%) in position 3. This way the equation giving the Intensity ratio (pump/probe) at the detector is:

$$\left(\frac{I_1}{I_2}\right)_{\text{detector}} = \frac{T_{\text{pcube}} \cdot T_{\text{cube30}} \cdot T_{\text{plate10}} \cdot R_{\text{cube10}}}{T_{\text{pcube}} \cdot T_{\text{cube30}} \cdot T_{\text{plate10}} \cdot R_{\text{cube30}}}, \quad (4.13)$$

whereas the intensity ratio at the Rb cell is:

$$\left(\frac{I_1}{I_2}\right)_{\text{cell}} = \frac{T_{\text{pcube}} \cdot T_{\text{cube30}}}{T_{\text{pcube}} \cdot T_{\text{cube30}} \cdot R_{\text{plate10}}}. \quad (4.14)$$

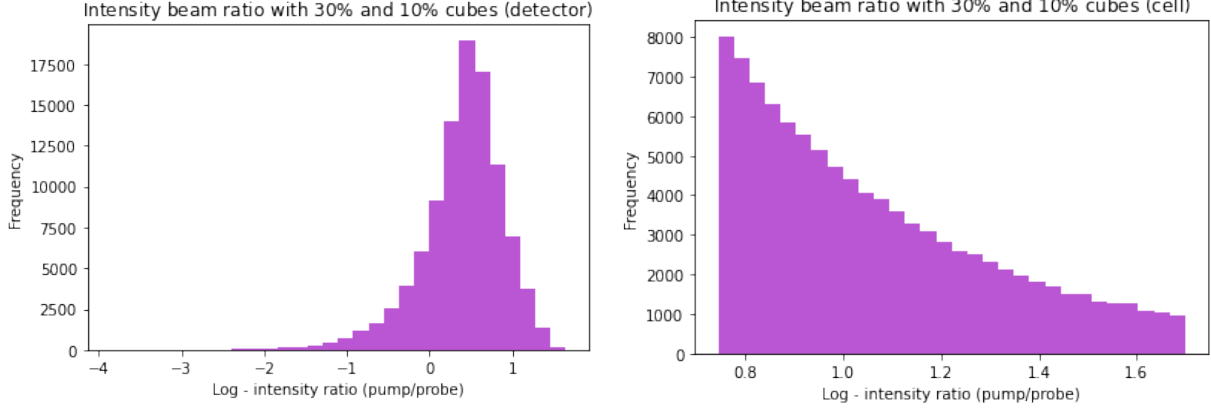


Figure (4.8) Intensity ratio (case 30 - 10)

### Case 10 - 30

For the second case, we consider that NPBS BS050 (with  $R\%=30\%$ ) is in position 3 and NPBS BS038 (with  $R\%=10\%$ ) in position 2. This way the equation giving the Intensity ratio (pump/probe) at the detector is:

$$\left(\frac{I_1}{I_2}\right)_{\text{detector}} = \frac{T_{\text{pcube}} \cdot T_{\text{cube}10} \cdot T_{\text{plate}10} \cdot R_{\text{cube}30}}{T_{\text{pcube}} \cdot T_{\text{cube}10} \cdot T_{\text{plate}10} \cdot R_{\text{cube}10}}, \quad (4.15)$$

whereas the intensity ratio at the Rb cell is:

$$\left(\frac{I_1}{I_2}\right)_{\text{cell}} = \frac{T_{\text{pcube}} \cdot T_{\text{cube}10}}{T_{\text{pcube}} \cdot T_{\text{cube}10} \cdot R_{\text{plate}10}}. \quad (4.16)$$

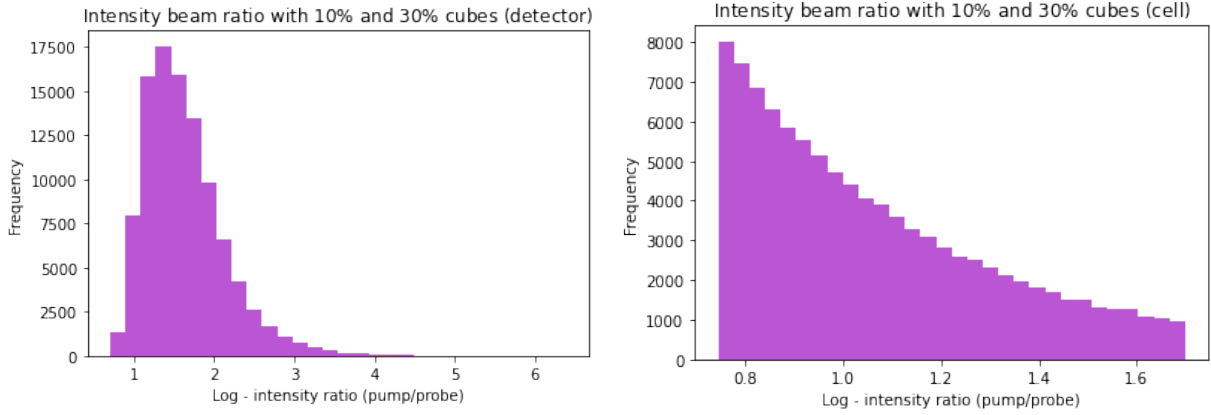


Figure (4.9) Intensity ratio (case 10 - 30)

### Case 70 - 10

For the third case, we consider that NPBS BS059 (with  $R\%=70\%$ ) is in position 2 and NPBS BS038 (with  $R\%=10\%$ ) in position 3. This way the equation giving the Intensity ratio (pump/probe) at the detector is:

$$\left(\frac{I_1}{I_2}\right)_{\text{detector}} = \frac{T_{\text{pcube}} \cdot T_{\text{cube70}} \cdot T_{\text{plate10}} \cdot R_{\text{cube10}}}{T_{\text{pcube}} \cdot T_{\text{cube70}} \cdot T_{\text{plate10}} \cdot R_{\text{cube70}}}, \quad (4.17)$$

whereas the intensity ratio at the Rb cell is:

$$\left(\frac{I_1}{I_2}\right)_{\text{cell}} = \frac{T_{\text{pcube}} \cdot T_{\text{cube70}}}{T_{\text{pcube}} \cdot T_{\text{cube70}} \cdot R_{\text{plate10}}}. \quad (4.18)$$

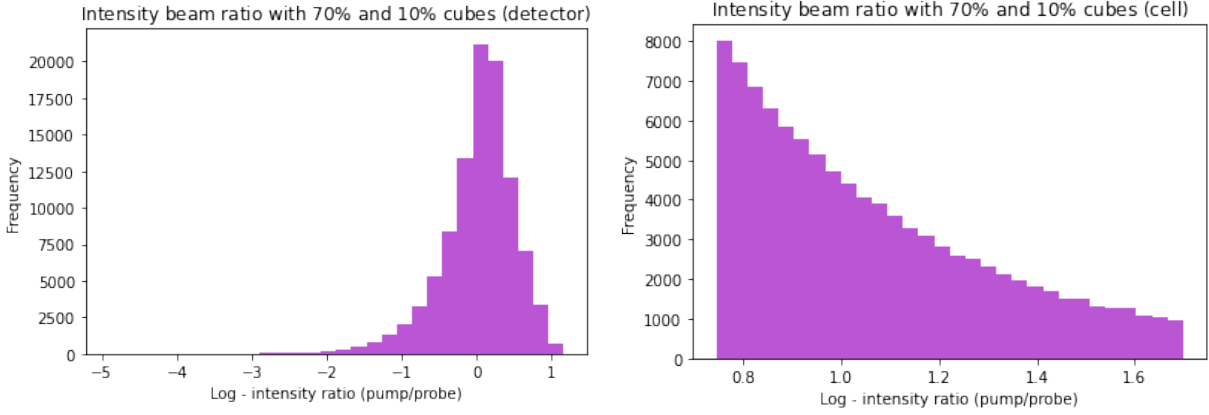


Figure (4.10) Intensity ratio (case 70 - 10)

### Case 10 - 70

For the fourth case, we consider that NPBS BS059 (with R%=70%) is in position 3 and NPBS BS038 (with R%=10%) in position 2. This way the equation giving the Intensity ratio (pump/probe) at the detector is:

$$\left(\frac{I_1}{I_2}\right)_{\text{detector}} = \frac{T_{\text{pcube}} \cdot T_{\text{cube10}} \cdot T_{\text{plate10}} \cdot R_{\text{cube70}}}{T_{\text{pcube}} \cdot T_{\text{cube10}} \cdot T_{\text{plate10}} \cdot R_{\text{cube10}}}, \quad (4.19)$$

whereas the intensity ratio at the Rb cell is:

$$\left(\frac{I_1}{I_2}\right)_{\text{cell}} = \frac{T_{\text{pcube}} \cdot T_{\text{cube10}}}{T_{\text{pcube}} \cdot T_{\text{cube10}} \cdot R_{\text{plate10}}}. \quad (4.20)$$

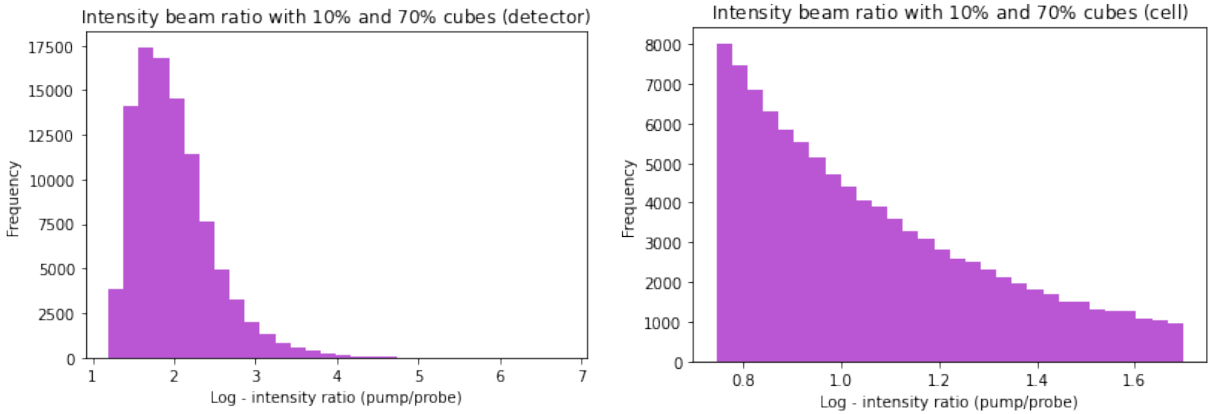


Figure (4.11) Intensity ratio (case 10 - 70)



### Case 70 - 30

For the fifth case, we consider that NPBS BS059 (with R%=70%) is in position 2 and NPBS BS050 (with R%=30%) in position 3. This way the equation giving the Intensity ratio (pump/probe) at the detector is:

$$\left(\frac{I_1}{I_2}\right)_{\text{detector}} = \frac{T_{pcube} \cdot T_{cube70} \cdot T_{plate10} \cdot R_{cube30}}{T_{pcube} \cdot T_{cube70} \cdot T_{plate10} \cdot R_{cube70}}, \quad (4.21)$$

whereas the intensity ratio at the Rb cell is:

$$\left(\frac{I_1}{I_2}\right)_{\text{cell}} = \frac{T_{pcube} \cdot T_{cube70}}{T_{pcube} \cdot T_{cube70} \cdot R_{plate10}}. \quad (4.22)$$

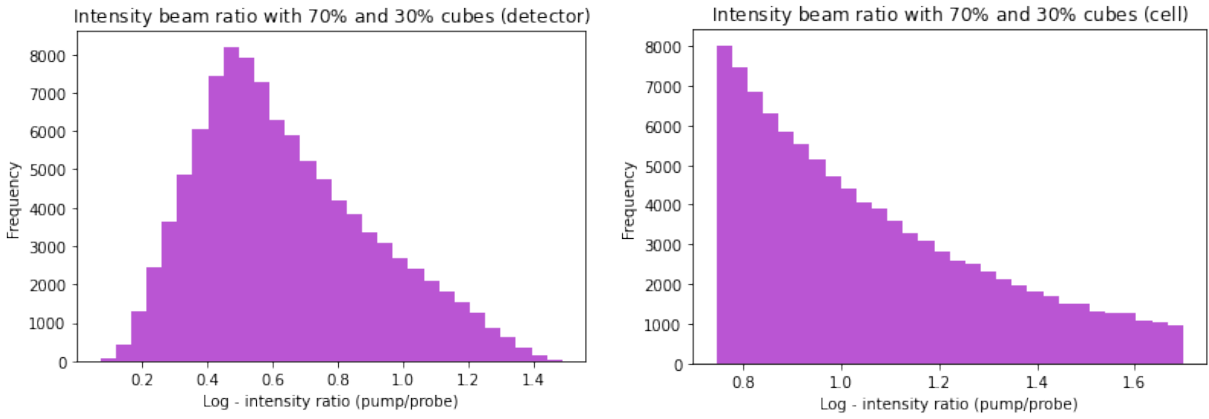


Figure (4.12) Intensity ratio (case 70 - 30)

### Case 30 - 70

For the sixth case, we consider that NPBS BS050 (with R%=30%) is in position 2 and NPBS BS059 (with R%=70%) in position 3. This way the equation giving the Intensity ratio (pump/probe) at the detector is:

$$\left(\frac{I_1}{I_2}\right)_{\text{detector}} = \frac{T_{pcube} \cdot T_{cube30} \cdot T_{plate10} \cdot R_{cube70}}{T_{pcube} \cdot T_{cube30} \cdot T_{plate10} \cdot R_{cube30}}, \quad (4.23)$$

whereas the intensity ratio at the Rb cell is:

$$\left(\frac{I_1}{I_2}\right)_{\text{cell}} = \frac{T_{pcube} \cdot T_{cube30}}{T_{pcube} \cdot T_{cube30} \cdot R_{plate10}}. \quad (4.24)$$

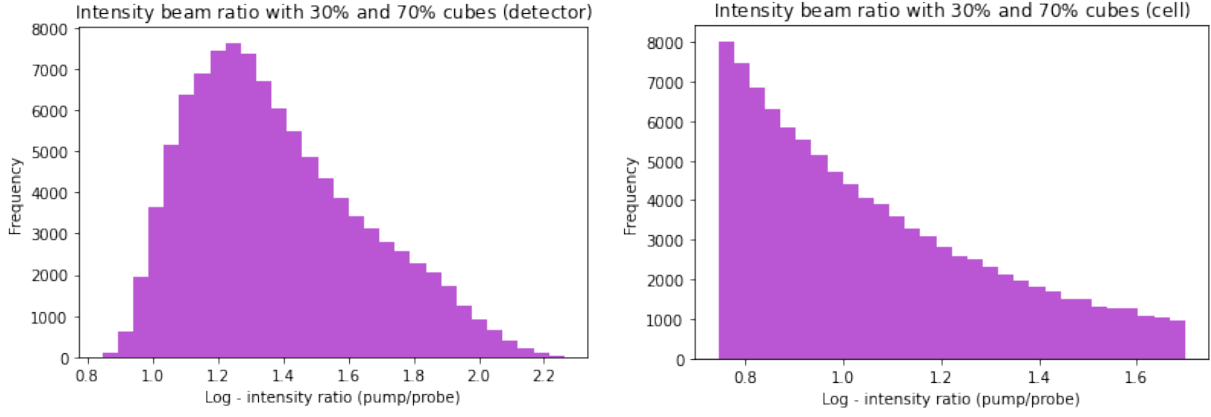


Figure (4.13) Intensity ratio (case 30 - 70)

## 4.4 Reflectivity and Transmittance Measurements

Once the components arrived at the lab, the actual values of R% and T% were measured, and the above distribution graphs delivered specific values for the intensity ratios, both at the detector and the cell. Moreover, an analysis for the lens selection, according to the preferable distance and diameter was conducted, using the measurements.

Table (4.3) R% and T% measurements of NPBS cubes and plate

Part Number	R	T
BS038	7.1%	89.2%
BS050	30.8%	67.8%
BS059	64.4%	35.0%
BSN05	11.9%	86.1%

## 4.5 Calculated Intensity Results

In order to calculate the final intensity ratio results, the values from table 4.3 are used in eq. (4.1) - eq. (4.24).

### 4.5.1 Intensity - setup no.1

For the setup no.1 (fig. 3.1), the results at the detector and the cell are presented below:

Table (4.4) Intensity ratio final results - setup no.1

Cases	$\log(I_1/I_2)$ - detector	$\log(I_1/I_2)$ - cell	$(I_1/I_2)$ - detector	$(I_1/I_2)$ - cell
30 - 10	0.34	1.02	2.17	10.56
10 - 30	1.73	1.26	53.77	18.28
70 - 10	0.02	1.43	1.04	26.92
10 - 70	2.34	1.84	217.78	68.60
70 - 30	0.94	1.26	8.74	18.28
30 - 70	2.16	1.84	143.43	68.60

### 4.5.2 Intensity - setup no.2

For the setup no.2 (fig. 3.2), the results are presented below:

Table (4.5) Intensity ratio final results - setup no.2

Cases	$\log(I_1/I_2)$ - detector	$\log(I_1/I_2)$ - cell	$(I_1/I_2)$ - detector	$(I_1/I_2)$ - cell
<b>30 - 10</b>	0.22	0.92	1.67	8.40
<b>10 - 30</b>	1.50	0.92	31.39	8.40
<b>70 - 10</b>	-0.10	0.92	0.80	8.40
<b>10 - 70</b>	1.82	0.92	65.63	8.40
<b>70 - 30</b>	0.54	0.92	3.46	8.40
<b>30 - 70</b>	1.80	0.92	15.13	8.40

## 4.6 Lenses specifications

As already mentioned in section 3.3.6, the following table includes the specifications of the purchased lenses, that will be used in the analysis in section 4.7

Table (4.6) Lens models specifications

a/a	Part Number	Diameter	Focal length
<b>Lens 1</b>	LD2568-B	9 mm	-9 mm
<b>Lens 2</b>	LD1357-B	12.7 mm	-50 mm
<b>Lens 3</b>	LD2746-B	6 mm	-6 mm
<b>Lens 4</b>	LD2060-B	12.7 mm	-15 mm

## 4.7 Lens distance analysis

In order to attenuate the power of the pump beam, so that the two beams have the same intensity at the detector, we need one lens (bi-concave or plano-concave). These kinds of lenses spread the beam, decreasing the intensity according to inverse square law:

$$\frac{I_1}{I_2} = \left(\frac{R_2}{R_1}\right)^2, \quad (4.25)$$

where  $I_1$  is the pump beam intensity,  $I_2$  the probe beam intensity,  $R_1$  the laser beam diameter before the lens and  $R_2$  the laser beam intensity after the lens. For better understanding, the diagram below is included:

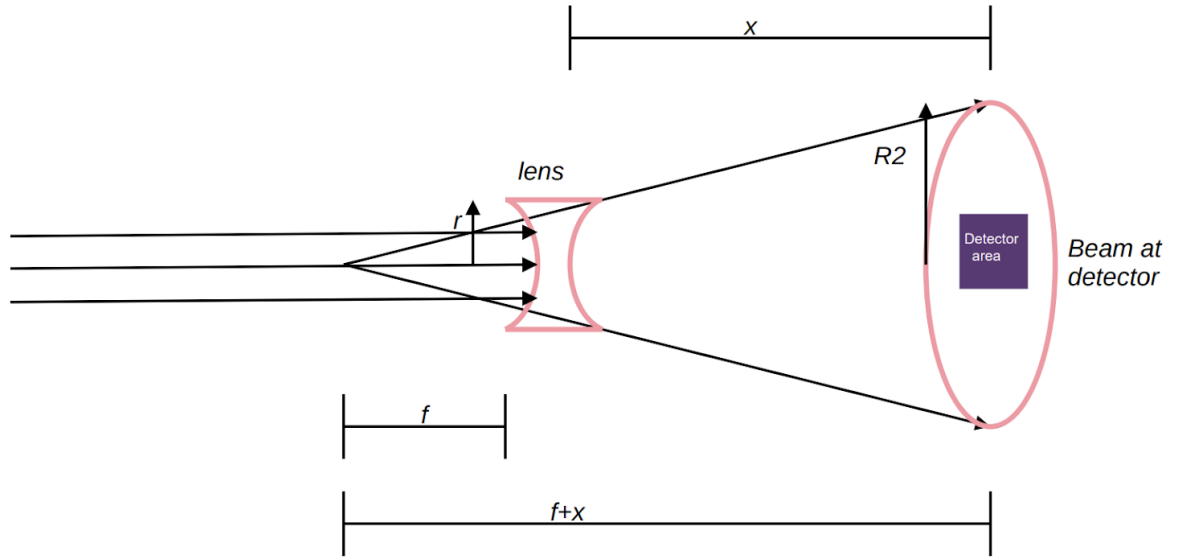


Figure (4.14) Lens arrangement

where  $r$  is the lens radius,  $R_2$  the beam radius after the lens at the detector,  $f$  the lens focal length and  $x$  the distance between the lens and the detector (here we consider  $x$  to be the distance between the lens and the PBS), which is also the desired result of this analysis.

For our calculations, we have considered that the initial laser beam diameter (before the lens) is  $R_1 = 3 \text{ mm}$ , and if we denote  $d = x + f$ , then the equation that gives us the distance  $x$  (using geometry) is:

$$x = R_1 \cdot \sqrt{\frac{I_1}{I_2}} \cdot \frac{f}{r} - f. \quad (4.26)$$

#### 4.7.1 Calculated Lens distance - setup no.1

In this section, the distance  $x$  will be calculated, for all lenses and for the setup no.1 (fig. 3.1), using the intensity ratios from section 4.5.1.

Table (4.7) Distance  $x$  - setup no.1

Cases	Lens 1	Lens 2	Lens 3	Lens 4
<b>30 - 10</b>	-0.16 mm	-15.21 mm	2.84 mm	-4.57 mm
<b>10 - 30</b>	35.00 mm	123.12 mm	38.00 mm	36.91 mm
<b>70 - 10</b>	-2.89 mm	-25.94 mm	0.11 mm	-7.78 mm
<b>10 - 70</b>	79.54 mm	298.42 mm	82.54 mm	89.48 mm
<b>70 - 30</b>	8.74 mm	19.81 mm	11.74 mm	5.93 mm
<b>30 - 70</b>	62.86 mm	232.76 mm	65.86 mm	69.79 mm

#### 4.7.2 Calculated Lens distance - setup no.2

In this section, the distance  $x$  will be calculated, for all lenses and for the setup no.2 (fig. 3.2), using the intensity ratios from section 4.5.2.

Table (4.8) Distance x - setup no.2

Cases	Lens 1	Lens 2	Lens 3	Lens 4
<b>30 - 10</b>	-1.25 mm	-19.51 mm	1.75 mm	-5.86 mm
<b>10 - 30</b>	24.61 mm	82.27 mm	27.61 mm	24.67 mm
<b>70 - 10</b>	-3.64 mm	-28.91 mm	-0.64 mm	-8.68 mm
<b>10 - 70</b>	39.61 mm	141.27 mm	42.61 mm	42.36 mm
<b>70 - 30</b>	2.16 mm	-6.08 mm	5.16 mm	-1.83 mm
<b>30 - 70</b>	14.34 mm	41.83 mm	17.34 mm	12.54 mm

## 4.8 Results and Discussion

### 4.8.1 Limitations on the distance

Table 4.7 and table 4.8 include the distance between the lens and the PBS (in mm), for every case and every setup. However, not all of them are acceptable. There are two limiting factors:

1. Lower limit: As can be seen from the drawings, there is also a quarter waveplate in the space between the lens and the PBS. From specs, its width is  $t = 3 \text{ mm}$ , and if we take into account a 5-mm distance before and after the waveplate (for design and printing reasons), then the total (together with an error margin) is  $\sim 10\text{mm}$ . This basically means that the lens cannot be at a distance less than 10mm, from the second PBS. So, the lower distance limit is :

$$x \geq 10\text{mm}. \quad (4.27)$$

2. Upper limit: In this case, the maximum distance lens-PBS is calculated. From fig. 3.1, we see that the distance between the mirror and the PBS, which can be the maximum one, is equal to the distance between the first and the second NPBS. Rb cell has a length equal to 20mm, and if we consider a 7-mm space before and after the cell, then the maximum distance for setup no.1 is  $\sim 34\text{mm}$ . Similarly, from fig. 3.2, the maximum distance is equal to the distance between the first and the second NPBS, now including both the cell (20mm) and the Plate Beamsplitter ( $t=3\text{mm}$ ), If we consider again, 7-mm space before and after the cell, and 5-mm space after the Plate Beamsplitter, then the maximum distance for setup no.2 is  $\sim 42\text{mm}$ . Briefly, the upper distance limit is:

$$x \leq 34\text{mm}, \text{no.1}, \quad (4.28)$$

$$x \leq 42\text{mm}, \text{no.2}. \quad (4.29)$$

### 4.8.2 Updated distance cases

So, if we take a look at the table 4.7 and table 4.8, we see that most of the values of x are rejected, and only a few remain as right solutions to our design.

Table (4.9) Distance x - acceptable values (setup no.1)

Cases	Lens 1	Lens 2	Lens 3	Lens 4
30 - 10	-0.16 mm	-15.21 mm	2.84 mm	-4.57 mm
10 - 30	35.00 mm	123.12 mm	38.00 mm	36.91 mm
70 - 10	-2.89 mm	-25.94 mm	0.11 mm	-7.78 mm
10 - 70	79.54 mm	298.42 mm	82.54 mm	89.48 mm
70 - 30	8.74 mm	19.81 mm	11.74 mm	5.93 mm
30 - 70	62.86 mm	232.76 mm	65.86 mm	69.79 mm

From the above, we see that only two values are acceptable for setup no.1, and one of them is really close to the lower limit, so it is really not a very good option. So for setup no.1, only the case with the 70% and 30% NPBS and lens LD1357-B (12.7 mm, -50 mm) will give the best signal result.

Table (4.10) Distance x - acceptable values (setup no.2)

Cases	Lens 1	Lens 2	Lens 3	Lens 4
30 - 10	-1.25 mm	-19.51 mm	1.75 mm	-5.86 mm
10 - 30	24.61 mm	82.27 mm	27.61 mm	24.67 mm
70 - 10	-3.64 mm	-28.91 mm	-0.64 mm	-8.68 mm
10 - 70	39.61 mm	141.27 mm	42.61 mm	42.36 mm
70 - 30	2.16 mm	-6.08 mm	5.16 mm	-1.83 mm
30 - 70	14.34 mm	41.83 mm	17.34 mm	12.54 mm

Again, we see that there are 3 acceptable values (yellow color), but pretty close to the limits, so for manufacturing reasons, they are also rejected. For setup no.2, there are 5 acceptable values: 3 for the case with the 10% and 30% NPBS, using lenses LD2568-B (9 mm, -9 mm), LD2746-B (6 mm, -6 mm) and LD2060-B (12.7 mm, -15 mm), and 2 for the case with 30% and 70% NPBS, using lenses LD2568-B (9 mm, -9 mm) and LD2746-B (6 mm, -6 mm).

In order to narrow down the options a bit more, we present some draft sketches of the acceptable cases, for better visualization. Moreover, for setup no.2, additional information can be found in Appendix.

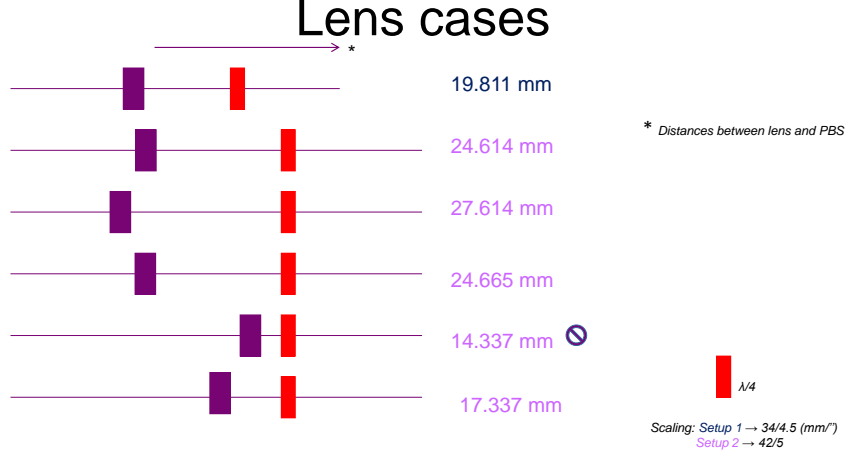


Figure (4.15) Visualization of acceptable cases

From fig. 4.15, one can notice that all cases can be designed and printed easily, except for the case "30 - 70", with lens LD2568-B. In general, for the final setups (including all cases), all three NPBS will be used, along with the lenses 1, 3 and 4 (table 4.6). Briefly, the acceptable cases, together with the intensity ratios, are presented below:

Table (4.11) Final cases for both setups

Setup no.1	Lens	Distance x	$(I_1/I_2)$ - detector	$(I_1/I_2)$ - cell
Case 70 - 30	1	19.81 mm	8.74	18.28
Setup no.2	Lens	Distance x	$(I_1/I_2)$ - detector	$(I_1/I_2)$ - cell
Case 10 - 30	1	24.61 mm	31.39	8.40
Case 10 - 30	3	27.61 mm	31.39	8.40
Case 10 - 30	4	24.67 mm	31.39	8.40
Case 30 - 70	3	17.34 mm	15.13	8.40

As a note, in order to have Doppler-free saturated absorption spectroscopy, it is important that the two beams have an intensity difference of a factor **5-15** in the cell, whereas, as already mentioned before, they should be nearly the same at the detector, meaning that the ratio should be close to **1**.

## 4.9 Magnetic field modulation analysis

In order to be able to get a clearer signal, one can use the *Zeeman effect*. By wrapping a wire around the cell, we create a coil, which then is connected to a function generator. By changing the frequency of the current in the coil, the induced magnetic field also changes, causing further splitting of the circular polarized beam components ( $\sigma+$  and  $\sigma-$ ). In this case, a magnetic field of *1 Gauss* or *2 Gauss* is preferable. It can be calculated from the following formula for solenoids:

$$B = \mu_0 \cdot \frac{N}{l} \cdot I, \quad (4.30)$$

where  $N$  is the number of wirings,  $I$  is the current from the function generator,  $l$  is the coil length and  $\mu_0$  is the permeability of free space. The available function generator at the lab can

offer a maximum current of  $I_{max} = 0.1A$ , so if we consider a safety factor of 1.4, and that the coil length is equal to that of the cell, then the number of wirings around the cell for  $B = 2G$  is **N = 46**, whereas for  $B = 1G$  is **N = 23** .



# Chapter 5

## Setup testing version

For the the testing of the setup, a first version was created, using mainly the components of chapter 3, among other materials, that will be discussed below.

### 5.1 Design of testing version

In order to test and check that the spectroscopy setup works before moving on with the 3D printing, another version was assembled in the lab, using methods for ultra stable optics in space projects, and the selected components, based on setup no.2. This basically means that a platform is used, onto which the components are glued at the right positions. A different detector is used instead of the transimpedance amplifier and the chosen photodiodes, so, the geometry and the optical lengths change slightly , as can be seen below:

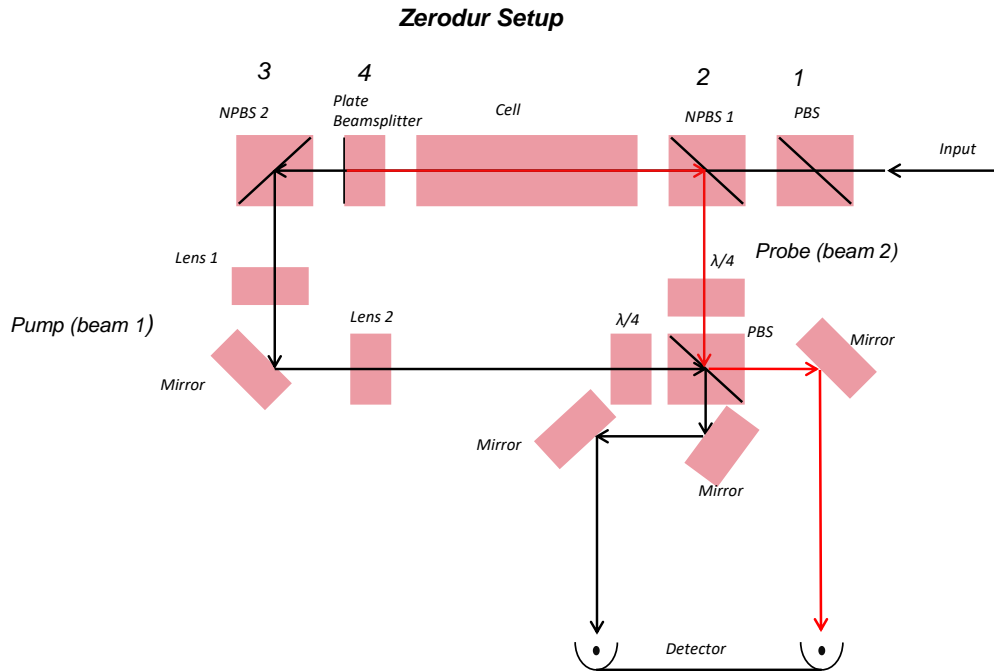


Figure (5.1) Setup version built for spectroscopy configuration testing

Setup no.2 was selected for this testing version, as analysis shows that it can offer more possible cases for obtaining the right signal (table 4.10). The difference from fig. 3.2 is the existence of one extra lens (with focal length  $f=50\text{mm}$ ), and three extra mirrors, as the optical lengths change. This is because of the geometry of the different detector used here, where the diodes appear to be in line next to each other. This poses a limit on the detector position, and also on the distance between the two beams after the second PBS, and the geometry shown above is calculated so that the beams have the same optical length after they leave the second PBS. Moreover, because the geometry changes after that, a combination of lenses is used to achieve the intensity equality of the two beams.

In particular, free-space balanced photodetector PDB210A/M (from Thorlabs) is used, with a distance of  $50.4\text{ cm}$  between the diodes. This, in combination with the platform size, leads to following geometric results:

- The mirror at the right of the 2nd PBS shall have a distance  $x_1 = 19.05\text{mm}$  from the PBS
- The two mirrors at the bottom of the PBS (as shown in the drawing) shall have a distance of  $x_2 = 25.4\text{mm}$ .
- The position of the middle mirror in the vertical axis does not affect the optical lengths.



Figure (5.2) PDB210A/M photodetector

## 5.2 Manufacturing of testing version

For the assembly of the testing version, a wide plate made of Zerodur is used as breadboard. Furthermore, all non-cubic elements are mounted to Zerodur cubes, using a melting Crystalbond adhesive at  $120^\circ\text{C}$ . For all the elements' mounts on the platform, a quartz wax glue is used, by heating it at  $60^\circ\text{C}$ . Two different adhesives are used, so that one can realign the optics by

heating the elements to the temperature at which the base melts, but the mirror stays attached to it. The testing assembly is presented below:

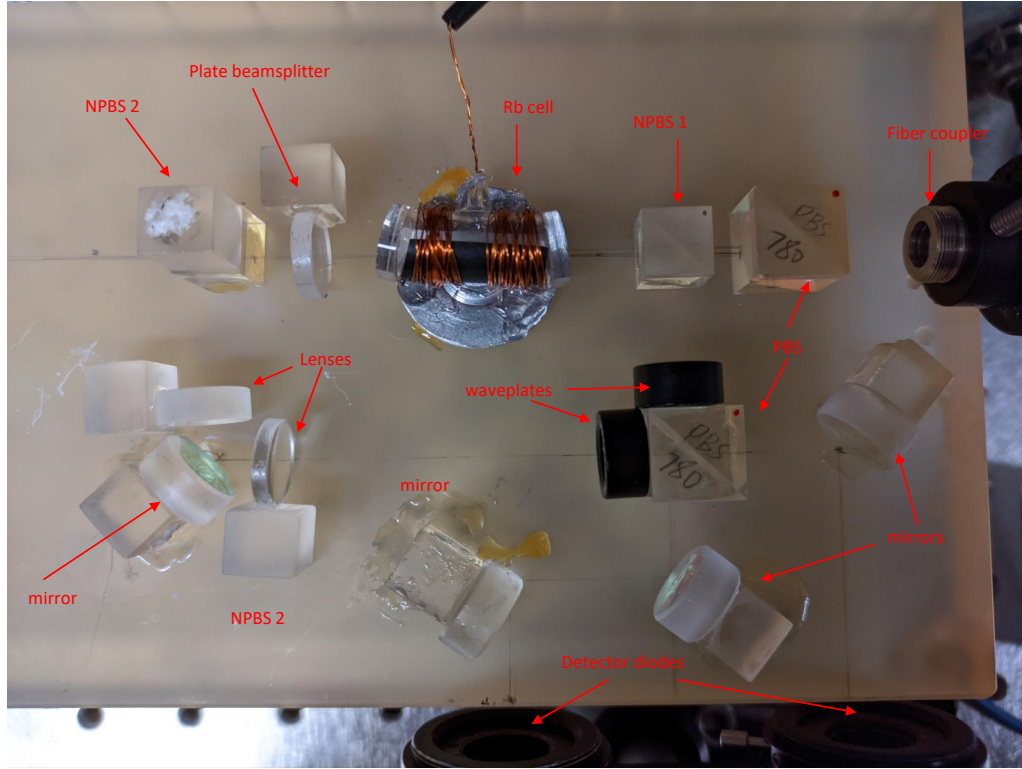


Figure (5.3) The testing version arrangement

The importance of the above setup lies to the fact that the majority of the components have previously been used in space experiments. More precisely, Zerodur is a space certified lithium-aluminosilicate glass-ceramic, that has often been used for mirror manufacturing in many telescopes, both on Earth and space (for example, in James Webb Space Telescope or OBST). Optical elements such as cubes, plates or mirrors can be used in space experiments, if the suitable testing procedures are followed. As a result, the assembled testing version of this project is an excellent platform that could possibly be used in space experiments at a later time, with only a few changes and additional tests.

## 5.3 Results

The input light intensity is determined by an external half waveplate before the fiber coupler (not shown in fig. 5.3), so that it is the same as the saturation intensity of Rb atoms at the cell,  $I = 1.67mW/cm^2$ . After assembling the setup, the signal from both beams is detected. In particular, using the second PBS and the waveplates, one can separate and control the detection of the  $\sigma$  and  $\pi$  components for both beams, and through the mirrors, they are led into the diodes. By placing the lenses at the right places, the intensities of the probe and the pump become the same and they can be subtracted. The final error signal is produced by demodulating the detector signal with a magnetic modulation, resulting in a derivative signal, the *error signal*. Moreover, the pump beam is added to the photodiodes in such a way that demodulated signals subtract. For this, it is important to ensure that the intensities of the

probe and pump beams match, so that the background is perfectly removed from the pump signal. The results are presented below:

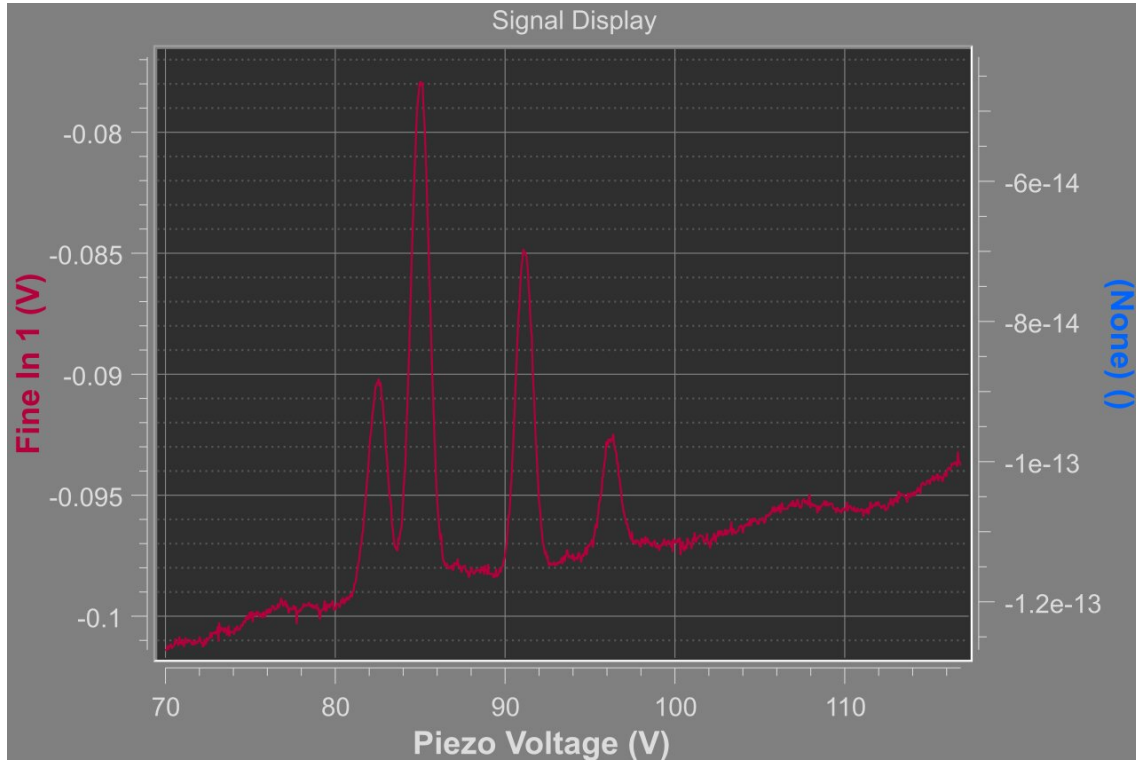


Figure (5.4) Absorption profile of the pump beam

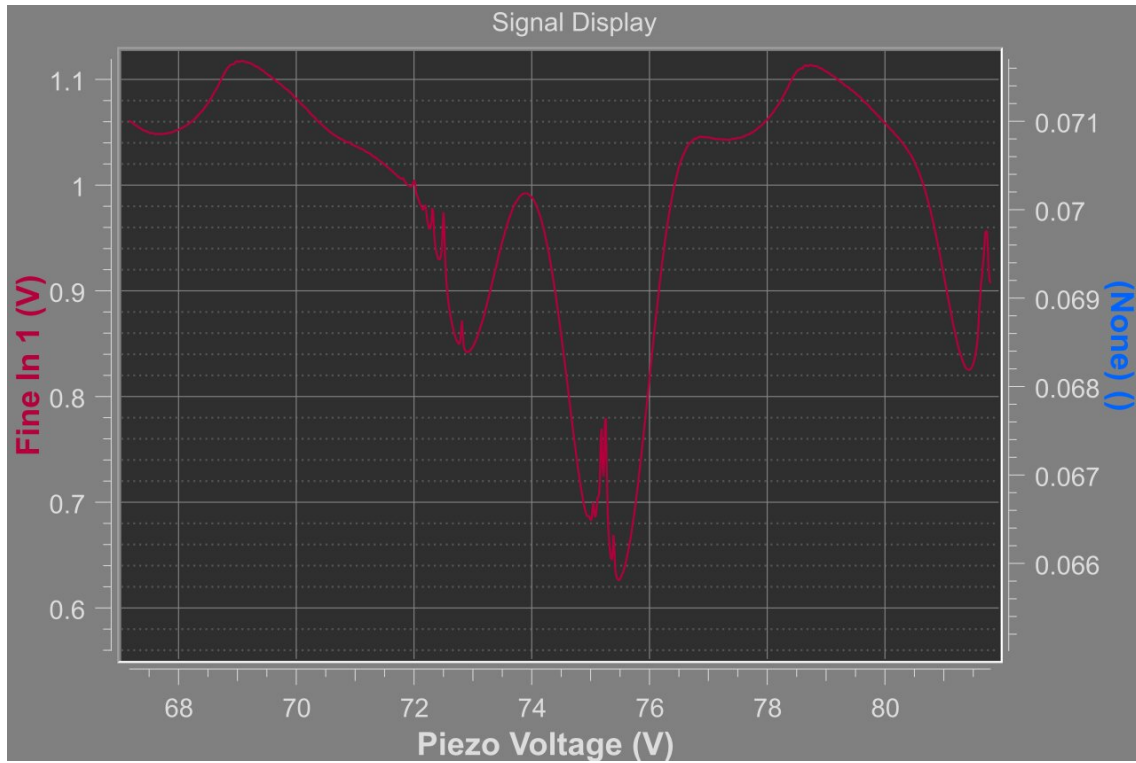


Figure (5.5) Doppler-free saturated spectroscopy of Rubidium. One can see some of the Lamb dips at the center of the main absorption dips

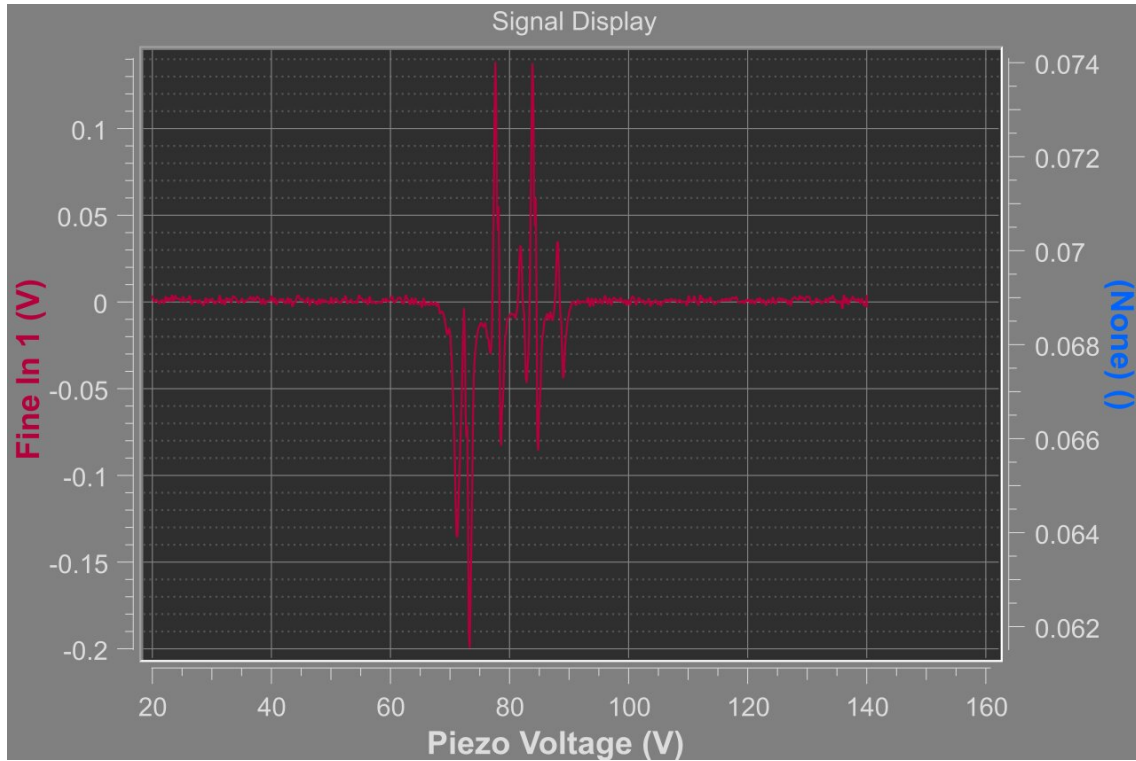


Figure (5.6) The resulting error signal, after the subtraction of the two beams and the modulation of the signal, through the Zeeman effect, that shifts further the  $\sigma+$  and  $\sigma-$  components, for both beams.

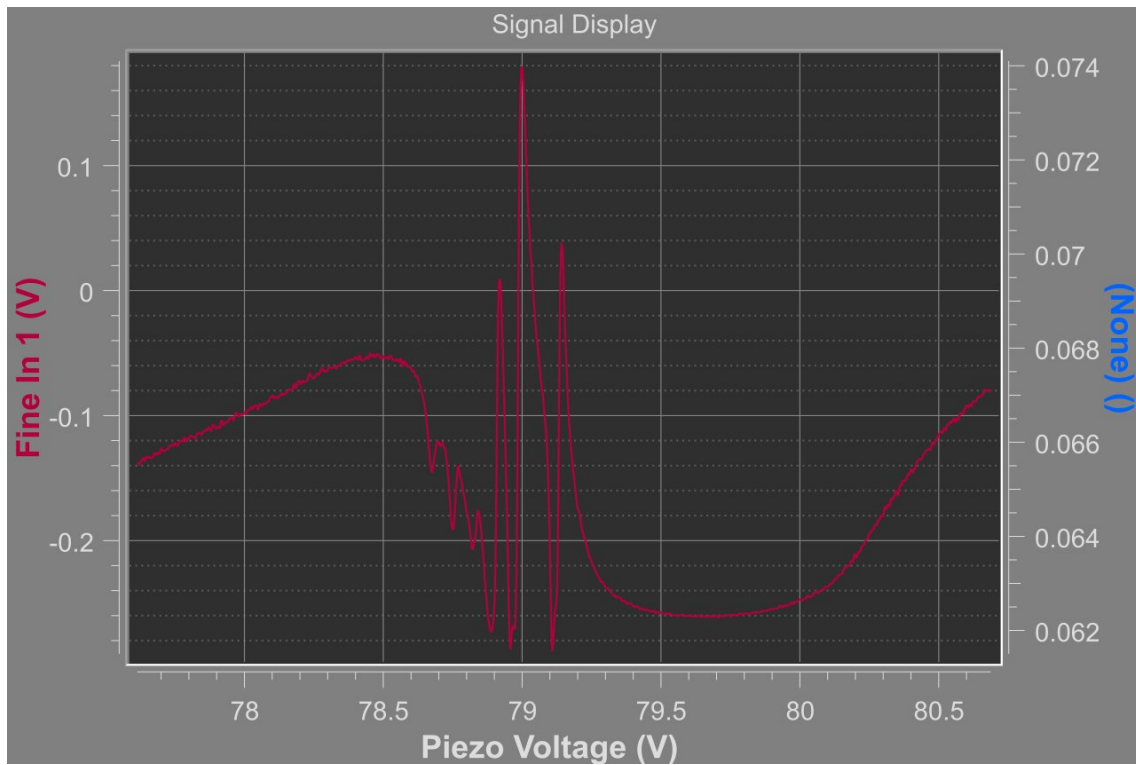


Figure (5.7) The resulting error signal for one transition (one of the four peaks shown in previous graph)

From the above, it becomes apparent that the configuration selected for the Rb spectroscopy for this project works very well, and the analysis has delivered some promising results, for the 3D printed model as well.

# Chapter 6

## 3D Module Design

### 6.1 Additive Manufacturing technique

Before moving on to the 3D design of the setup, it is useful to mention some basic information about the technique of Additive Manufacturing (AM), or *3D Printing*. With this procedure, production is done layer by layer, and there is a wide variety of materials that can be used. A more precise definition mentions that *"three-dimensional printing (also known as Rapid Prototyping) is the process of making 3D objects from 3D modeled data in progressive layers, and it is currently being promoted as the spark of new industrial revolution"* [4]. Before the additive manufacturing, there is the step of the digital manufacturing, which is actually the manipulation of the object in its digital form. Then, it is shaped by the material addition, that usually happens in the sub-mm scale. 3D printing is quite important, as it helps manufacturers achieve lower costs, lead times and lighter, stronger designs, while avoiding complex assemblies and utilizing up to 90% of the materials at the same time.

#### 6.1.1 Materials

In general, there are different types of technologies, that handle different materials in a different way, for example sand, plastic, metal, ceramics, paper or bio-materials. Nowadays, the most common ones are Nylon, Acrylonitrile Butadiene Styrene (ABS) or Polylactic Acid (PLA). Materials can be found in different states, such as filament, powder, pellets, granules or resin.

#### 6.1.2 Processes

The basic 3D printing processes are presented below:

- Stereolithography
- Digital Light Processing (DLP)
- Laser sintering / Laser melting
- Extrusion / Fused Deposition Modelling (FDM) / Freeform Fabrication (FFF)
- Inkjet
- Electron Beam Melting (EBM)

The most common process is the extrusion, where thermoplastic filament is extruded through a heated extruder to create detailed layers of the object.

### 6.1.3 3D printing in space

3D printing technology has also entered the space industry, in many interesting ways. Recently, European Space Agency started experimenting on creating 3D printed models on the International Space Station (ISS). Moreover, a great number of space projects aim at developing 3D printed structures for lunar habitation, and Mars exploration. 3D printing is also used for satellite, thrusters, rocket engines, food and astronaut clothing production, that will play an important role in the near future.

## 6.2 Computer-Aided Design (CAD)

Computer-Aided Design (CAD) is the best way to digitally manufacture an object, before physically produce it via Additive Manufacturing. CAD technique, as it is already mentioned in its name, uses computers for the creation, modification or analysis of an object's 2D or 3D design. This way, better quality and documentation are achieved, along with more thorough design databases.

Next, we are going to present and compare three of the most wide-used CAD software tools in today's industry.

1. Inventor (by Autodesk): Mostly used for mechanical design, documentation and product simulations. It allows for rapid assembly reconfigurations (use of gears, cams or bolted connections from library), demands less lead time in engineering and design, even by 20%, while offering cloud integration, updates and simulation of kinematic parts. However, it is available only for Windows OS. Inventor is a more specialized tool, that connects design, engineering and manufacturing, and a better choice for highly complex assemblies, whole mechanics projects and stress tests.
2. AutoCAD (by Autodesk): Used for both 2D and 3D program designs, it is a very good solution, offering high precision and accuracy. It is suitable for 2D sketches and documentation, allowing for comments to be added as well. It is compatible with iOS and Windows, but not Linux OS. It is mainly used for architectural projects, mapping and whole constructions, but not mechanical engineering projects.
3. SolidWorks (by Dassault Systemes'): The user can begin with a 2D sketch and then expand and part extrude into 3D using SolidWorks tools. One can also work on very large assemblies (with millions of components), and have the ability for different, various tests. It is one of the oldest and tested CAD software tools, and the most used one in aerospace industry.

*Inventor* appears to be the most suitable option for the current project thesis. The reasons for that, as mentioned above, is that it offers the best solution for mechanical design and product simulations, using less time. Therefore, Autodesk Inventor Professional versions 2021 and 2022 will be used for the setup design, provided by University of Crete and IESL-FORTH, respectively.



## 6.3 Setup Dimensions

As a first step to the 3D design of the module, it is important to define the dimensions of each setup version (fig. 3.1, fig. 3.2).

Table (6.1) Dimensions for setup no.1

Setup no.1	Components	Components + in between space (mm)	Total
<i>Length</i>	Fiber Coupler - PBS - NPBS - Rb cell - NPBS - Plate Beamsplitter	17.00 + 5.00 + 10.00 + 5.00 + 10.00 + 7.00 + 20.00 + 7.00 + 10.00 + 5.00 + 3.00 + 11.00 (margins)	110.00 mm
<i>Width</i>	Rb cell - PBS - Photodiode	10.00 + 5.00 + 10.00 + 5.00 + 10.00 (with margins and photodiode)	40.00 mm
<i>Height</i>	Mirror/Plate Beamsplitter (larger than the rest)	12.70 + 7.30(margins)	20.00 mm

Table (6.2) Dimensions for setup no.2

Setup no.2	Components	Components + in between space	Total
<i>Length</i>	Fiber Coupler - PBS - NPBS - Rb cell - Plate Beamsplitter - NPBS	17.00 + 5.00 + 10.00 + 5.00 + 10.00 + 7.00 + 20.00 + 7.00 + 3.00 + 5.00 + 10.00 + 11.00 (margins)	110.00 mm
<i>Width</i>	Rb cell - PBS - Photodiode	10.00 + 5.00 + 10.00 + 5.00 + 10.00 (with margins and photodiode)	40.00 mm
<i>Height</i>	Mirror/Plate Beamsplitter (larger than the rest)	12.70 + 7.30(margins)	20.00 mm

We notice that the two setups have the same dimensions

$$(L \times W \times H) = 110.00 \times 40.00 \times 20.00 \text{ mm}$$

## 6.4 Project Design and Prototyping Flow Graph

After the analysis and the definition of the best cases that one can test for the module, the testing version design and manufacturing took place, as shown in chapter 5. Another step that follows, is of course the 3D CAD and printing. As soon as a setup version is printed, the selected components are integrated (a variety of different setups will be printed, depending on the allowed cases of table 4.9 and table 4.10). After this, the whole setup is tested, in order to derive the desired error signal, and one can be able to lock the laser (laser stabilization). In case of errors, updates are necessary, and re-printing follows, along with all next steps. Once the right signal is obtained, the final module is then ready.

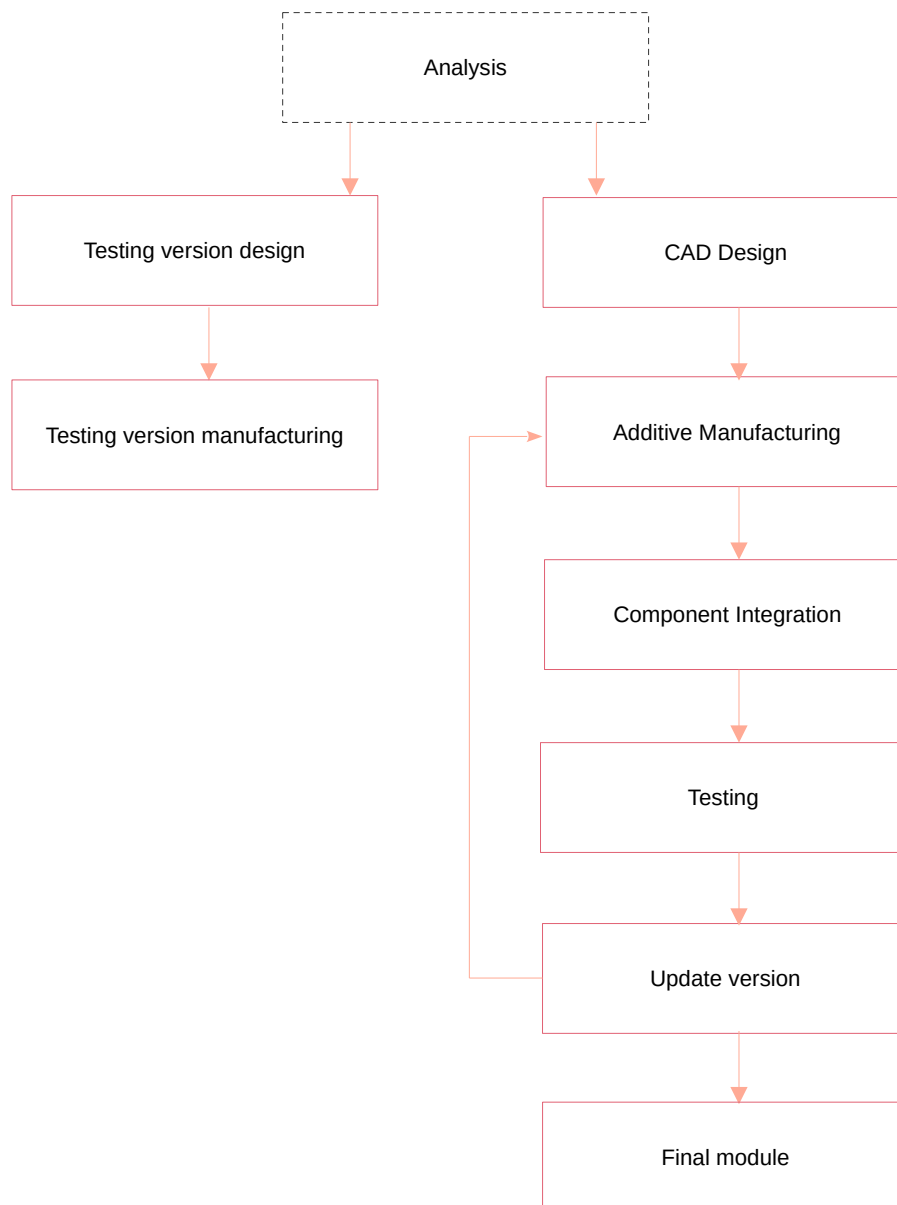


Figure (6.1) Flow graph of the module design and prototyping

## 6.5 3D Setup

In the following sections, the design for setup no.1 will be presented, along with comments related to the CAD properties. The material "*ABS plastic*" was selected, as it is a common choice for simple products like this. In addition to this, little holes - with radius  $r = 1\text{ mm}$  - are added to the corners of the push-fit slots of the components, in order to reduce the stress on them, and help with the manufacturing. The horizontal holes, made for the laser beams, have a radius of  $3\text{ mm}$ , the output slots are designed for the pin photodiodes, whereas the input slot is designed for part of the fiber coupler.

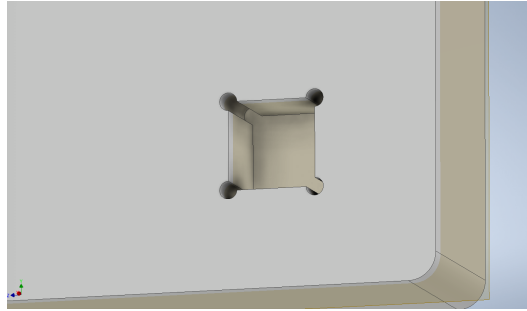


Figure (6.2) Detail of the design - corner-holes

Based on fig. 3.1, the Inventor preliminary 3D design of setup no.1 is:

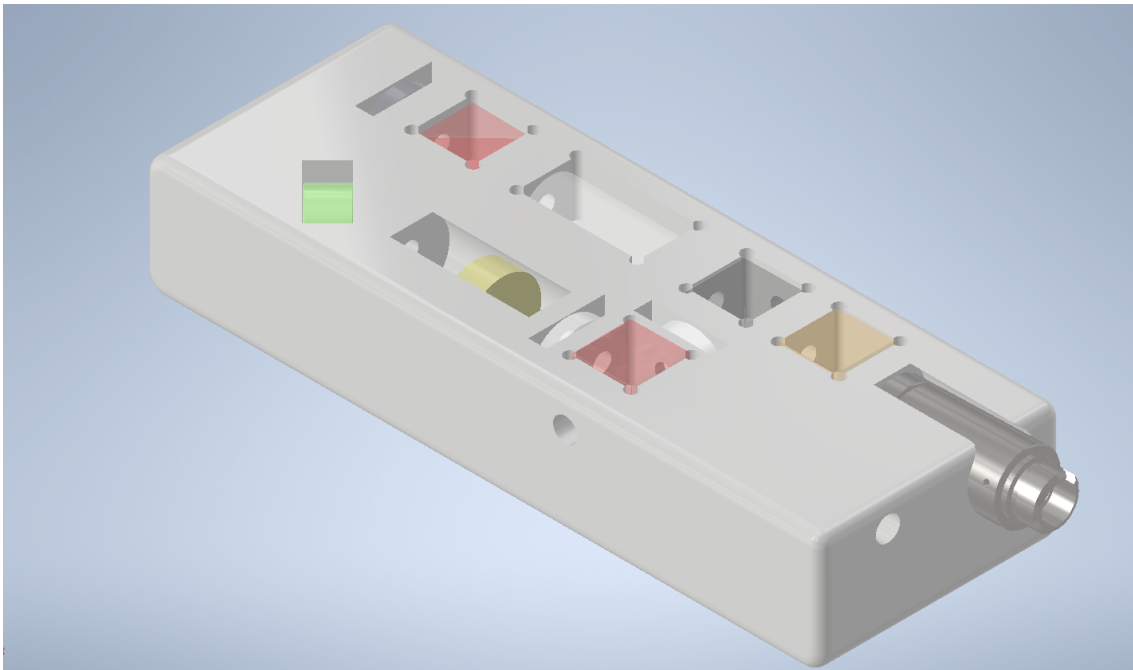


Figure (6.3) Setup no.1 CAD, with components



Figure (6.4) Setup no.1 CAD, with components - top view

Based on fig. 3.2, the 3D design of setup no.2 is very similar to the above one, and the only difference is the switched positions between the second NPBS and the Plate Beamsplitter. More figures of the CAD can be found in Appendix.

A 3D printed mockup version is shown below. The material used is *PLA*, and the total setup mass is  $32g$ .



Figure (6.5) 3D printed mockup of the setup, compared to a 20-cent coin

Finally, the mock-up is compared to the normal spectroscopy arrangement that exists in our lab and the size difference becomes obvious.

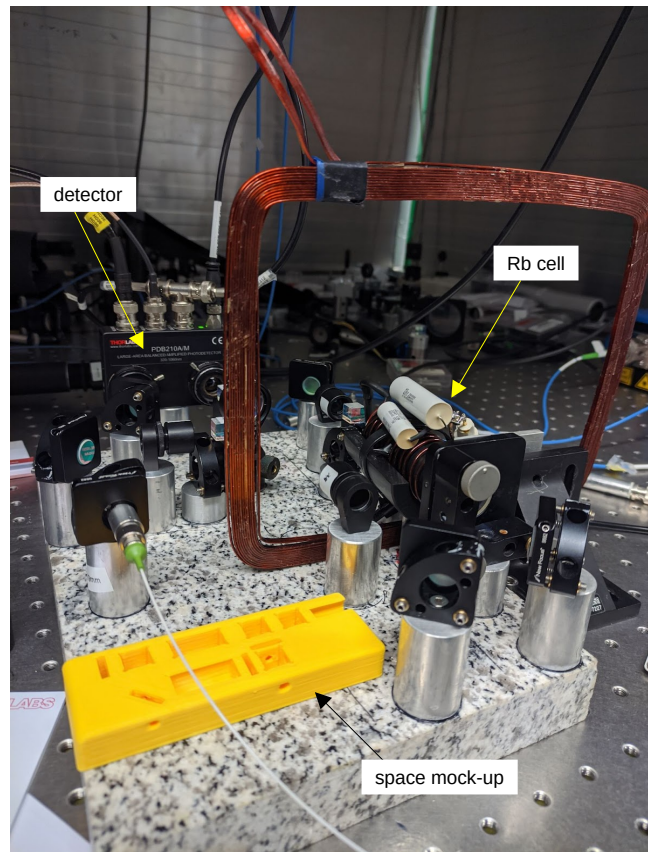


Figure (6.6) The mockup compared to our lab's normal-size spectroscopy arrangement

# Conclusion

In this thesis, we attempt to design a modern module, suitable for laser stabilization in space applications. The best method for that is the *Doppler-free Spectroscopy*, also known as *Saturated Absorption Spectroscopy*. A short introduction about lasers and laser spectroscopy is first presented, together with the importance of the current project. Doppler-free spectroscopy could be used widely in space experiments, where there is high need of stable frequency pulses. Consequently, we try to build a 3D setup, by printing it, which will combine great effectiveness and results, with small cost and size. In order to be accurate with the design, all the components, along with parts used for redundancy, are selected beforehand, after conducting a thorough trade-off analysis. Once the components are selected and ordered, one moves on with the analysis, so as to determine the exact combination of Non-Polarizing Beamsplitters that offers the best results. For this reason, the ratio of the intensity of the two beams (pump and probe) in the experiment is studied, both at the Photodetector and the Rubidium cell. Actual measurements of the final components' Reflectivity and Transmittance allow us to have far better results, and decide which lenses are most appropriate to use, and at what distance. Finally, there are several cases/setup versions, that can be manufactured, before choosing the best one. Then, a testing version is assembled, in order to check that the configuration selected for this project works, and the final results are obtained with great accuracy. Next, a 3D design is created, using the CAD tool *Inventor*. At the time of this thesis, the design was at a preliminary stage, and a draft model is included here. More details and analysis will follow at a later time, right before the 3D printed manufacturing and module production. Next steps also include the integration of components into the printed setup, and the test of the whole module using the available facilities. Lastly, when the final setup is produced, an attempt for commercialization will follow.

# Appendix

## A1. Lens cases (setup no.2)

Below is an additional sketch showing the lens positions, according to the final cases in table 4.11, from two different views. Only three cases for the second setup are included.

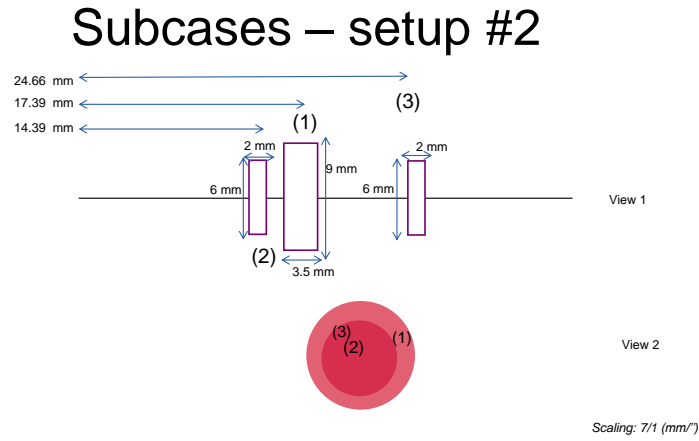


Figure (6.7) Visualization of acceptable cases for setup no.2 - positions of lenses (left view and front view respectively)

## A2. Inventor design for 3D printing

### Setup no.1

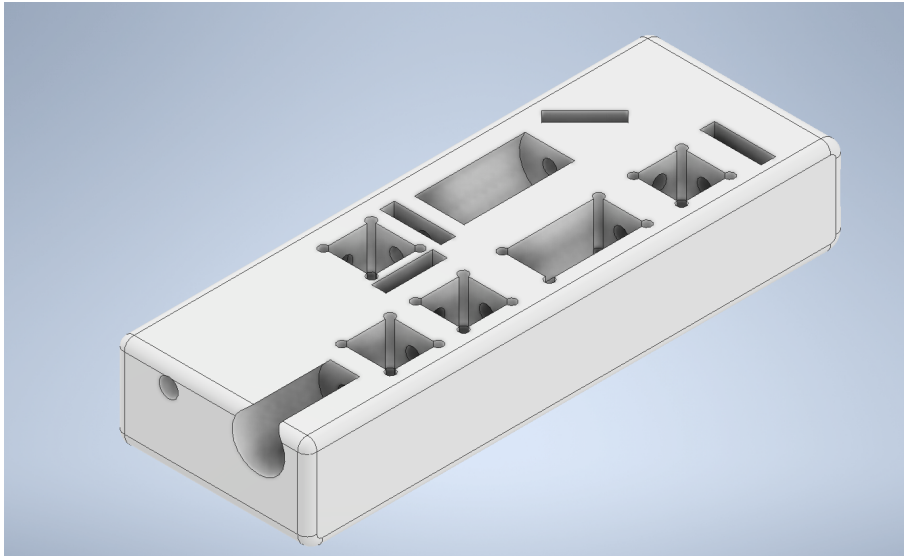


Figure (6.8) 3D design of setup no.1

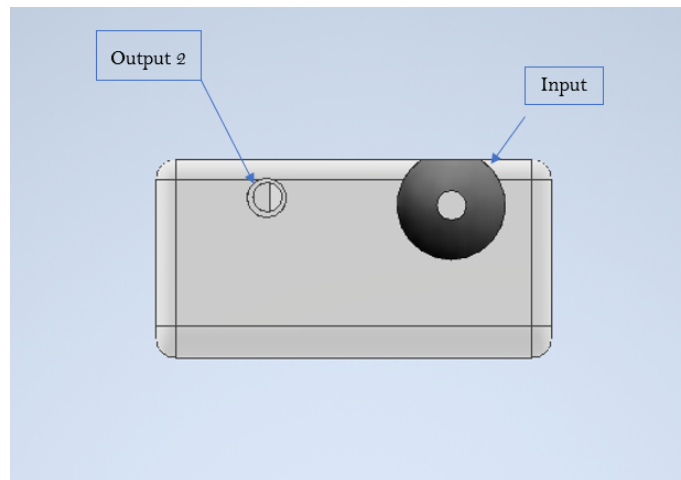


Figure (6.9) Front view of module no.1

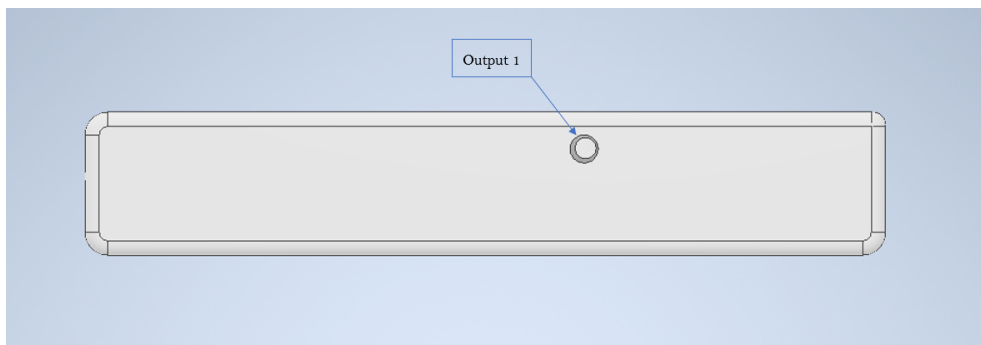


Figure (6.10) Left view of module no.1



Setup no.2

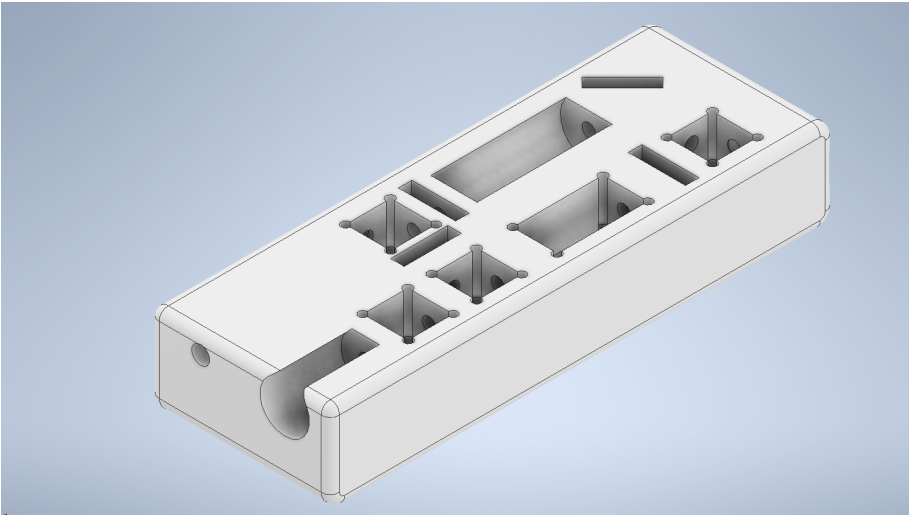


Figure (6.11) 3D design of setup no.2

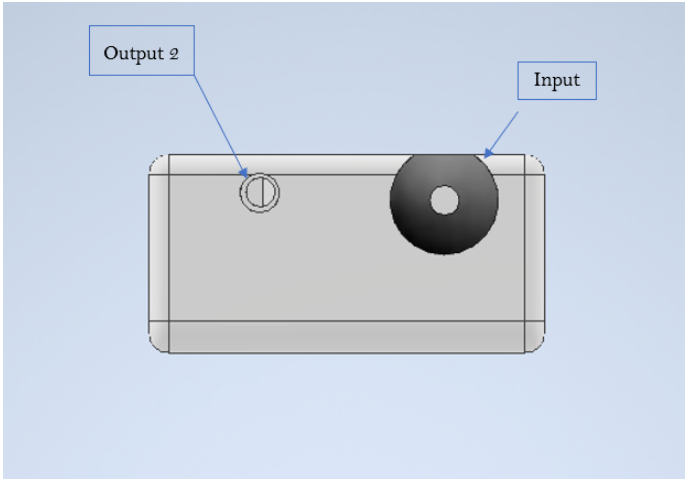


Figure (6.12) Front view of module no.2

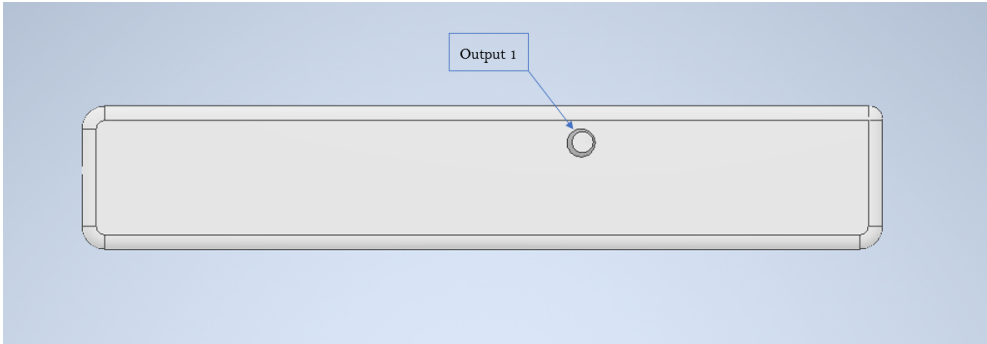


Figure (6.13) Left view of module no.2

# Bibliography

- [1] W. Demtröder. *Laser Spectroscopy*. Number 4. Springer Berlin, Heidelberg.
- [2] P. Examilioti. Double compensated sub-Doppler spectroscopy for ultra-cold atom experiments, 2021.
- [3] G. S. Giri. Laser spectroscopy of rubidium. 2016.
- [4] T. Hasan Masood Siddique, I. Sami, M. Zohaib Nisar, M. Naeem, A. Karim, and M. Usman. Low Cost 3D Printing for Rapid Prototyping and its Application. *arXiv e-prints*, page arXiv:1911.10758, Nov. 2019.
- [5] S. H. Madkhaly, L. A. Coles, C. Morley, C. D. Colquhoun, T. M. Fromhold, N. Cooper, and L. Hackermüller. Performance-Optimized Components for Quantum Technologies via Additive Manufacturing. *PRX Quantum*, 2(3):030326, Aug. 2021.
- [6] S. H. Madkhaly, N. Cooper, L. Coles, and L. Hackermüller. High-performance, additively-manufactured atomic spectroscopy apparatus for portable quantum technologies. *Optics Express*, 30(14):25753, July 2022.
- [7] D. Steck. Rubidium 87 d line data. 2003.
- [8] O. Svelto. *Principles of Lasers*. Number 5. Springer New York, NY.